CHALMERS
UNIVERSITY OF TECHNOLOGY

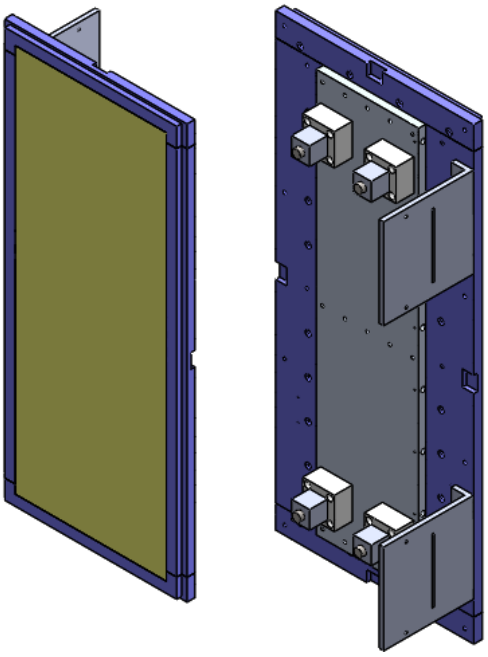

Design of instrumented end-wall for heat transfer measurements in a low-speed linear cascade and flow measurements

Master's Thesis in Solid and Fluid Mechanics

Saül Josep Llácer Navarro

Department of Applied Mechanics
Division of Fluid Dynamics
Chalmers University of Technology
Göteborg Sweden, 2014

Master's Thesis [2014 : 77]

Master's Thesis 2014:77

Design of instrumented end-wall for heat transfer measurements in a low-speed linear cascade and flow measurements

Master's Thesis

Saül Josep Llácer Navarro

Department of Applied Mechanics
Division of Fluid Dynamics
Chalmers University of Technology
Göteborg, Sweden, 2014

Design of instrumented end-wall for heat transfer measurements in a low-speed linear cascade and flow measurements
Master's Thesis
Saül Josep Llácer Navarro

Master's Thesis 2014:77
ISSN: 1652-8557

Department of Applied Mechanics,
Division of Fluid Dynamics
Chalmers University of Technology
Se-412 96 Göteborg, Sweden
Phone +46-(0)31-7721400
Fax: +46-(0)31-180976

Printed at Chalmers Reproservice
Göteborg, Sweden 2014

Saül Josep Llácer Navarro

Master's Thesis

by

Saül Josep Llácer Navarro
saul@student.chalmers.se
Department of Applied Mechanics
Division of Fluid Dynamics
Chalmers University of Technology

Abstract

The main purpose of this study is to design an instrumented end-wall to study the heat transfer mechanisms and flow measurements in Outlet Guided Vanes (OGVs) section in a linear cascade located at Chalmers University of Technology in order to understand the thermal interaction between the OGVs, end-walls and the air flow.

The design is conducted using Computer-Aided Design(CAD), the CAD software used in this project is SolidWorks. Furthermore, an optimization of the design has been performed using SolidWorks and Matlab in order to minimize the heat transfer measurement error during the experiments. The data acquired with these studies can be used for CFD validation purposes or for future design modifications of the OGVs or endwalls as the coolant needed or the materials that can be used.

In addition, flow measurements in a low-speed linear cascade has been performed to understand the fluid behaviour in this section. The data obtained in these experiments can be compared with other similar experiments and with CFD simulations.

Contents

Acknowledgement

The thesis was done in the Department of Applied Mechanics at the Division of Fluid Dynamics at Chalmers University of Technology in Göteborg - Sweden. The work was supervised by Docent Valery Chernoray and the Ph.D. student Borja M. Rojo Perez.

First, I would like to thank my parents for misunderstanding all my ideas, but nodding and smiling at the same. They were so important for me for their support and for helping me to finance my studies. Without their help, I would never have been able to perform my studies.

I would like to express my thanks and gratitude to Professor Valery Chernoray for continuous support, the helpful advice, and the valuable guidance throughout the work. Furthermore, he kindly assumed the responsibilities of my thesis.

I would like to express my thanks and gratitude to the Ph.D. student Borja M. Rojo, who gave me this opportunity offering me this master thesis. Despite that, he deserves a Nobel Prize for putting up with me. He was able to help me, teach me and give me his advice even on Sundays or late at night, and most of all, for giving me his friendship.

I thank all the professors, Ph.D students and members at the Fluid Dynamics Division, they created a very good environment for me to study and work every day. I will not forget their patience to teach me and have every single day "Fika". In special thanks to Angel Barrachina, who made his Master Thesis next to me at the Linear Cascade helping each other with our experiments. I do not would like to forget to thanks Carlos Jimenez, project assistant, who helped us in every technical aspect even improving the IR camera software.

All of this will not be possible without my flat mates Pilar Dominguez, Casandra Zamorano and Carlos Villanueva. I would like to thank them for taking my mind off the thesis when it went wrong or at the sad Swedish winter. They made me happy every second I was at home with them, I really appreciate it.

I also would like to thank Chalmers University of technology and GNK aerospace. They supported this thesis, without them nothing of this would be possible.

Finally, I would like to express my special thanks to my friends for their patience and encouragement.

1

Introduction

Due to the necessity to develop an efficient and accessible technology, it becomes necessary to study the processes taking place in each technology. The efficiency in a heat engine depends on the temperature difference between the heat source and the cold source, obtaining higher efficiencies while the temperature difference is higher. In this case, the experiment was focused in the study of fluid flow through a vane situated inside a low-speed linear cascade. The aim of this experiment is to understand the complex processes involved inside the engine exit structure (EES) of an aero-engine.

It is of special interest the heat transfer phenomena involved in this section, especially local high heat transfer coefficient to avoid high thermal stresses on the end-walls on OGVs, causing early damage to the components. Therefore, having the possibility of predicting the heat transfer coefficients in this section can lead to an improvement of the design, such as which material is the most suitable for the EES as well as the design of cooling flow for the OGV if needed.

Main objective

The main goal is to design an instrumented window and minimize the error measuring the heat transfer coefficient on a vane surface and on the end-wall. Furthermore, the fluid's behaviour at the linear cascade is analysed using the information acquired by pressure measurement techniques. This study has been adapted from the experiment in Rojo et. al. (2014), modifying aspects such as the possible gaps of air between the layers of his instrumented window.

1.1 Basic Background

1.1.1 Gas turbine description

A gas turbine is a heat engine where the combustion is situated within, it is a type of internal combustion engine. The turbine works continuously. It consists of several parts:

Fan. Here is where the compression starts. Air stream is divided in two, the primary flow and the bypass air. The first one goes through the axial compressor and subsequently to the combustor.

Compressor. At this point the air enters in order to be compressed adiabatically to the pressure of combustion through various stages of compressors rotating in the same direction of the fan. Here is where the temperature increases due to increased pressure. Higher pressure ratios leads to higher efficiencies.

Combustor. Here the chemical energy is added by the fuel, it is injected thereby producing the combustion, resulting in a supply of heat (Q) to the heat engine. The combustion process takes place at constant pressure thus very high temperatures are reached, also the volume is increased.

Turbine. This stage is the expansion phase. The turbine extracts energy from the exhaust gases from combustor by making the blades spin. In a jet engine, which is a type of a gas turbine, the energy extracted by the turbine is used to drive the compressor by linking the compressor and the turbine by the central shaft. The turbine takes some energy out of the hot exhaust, but the flow leaving the turbine is at a higher pressure, temperature and velocity than the free stream flow.

Exhaust Duct. The air exits through the rear of the engine, this is collected, straightened and accelerated by the narrow walls of the nozzle. Most of the thrust comes from the velocity difference between the velocity of the free stream and the exhaust gases.

Bypass flow duct. That concentrically surrounds the core engine. Its internal and external walls are carefully shaped to minimize the energy loss of the bypass air flow and optimizing its mixing with the primary exhaust flow.

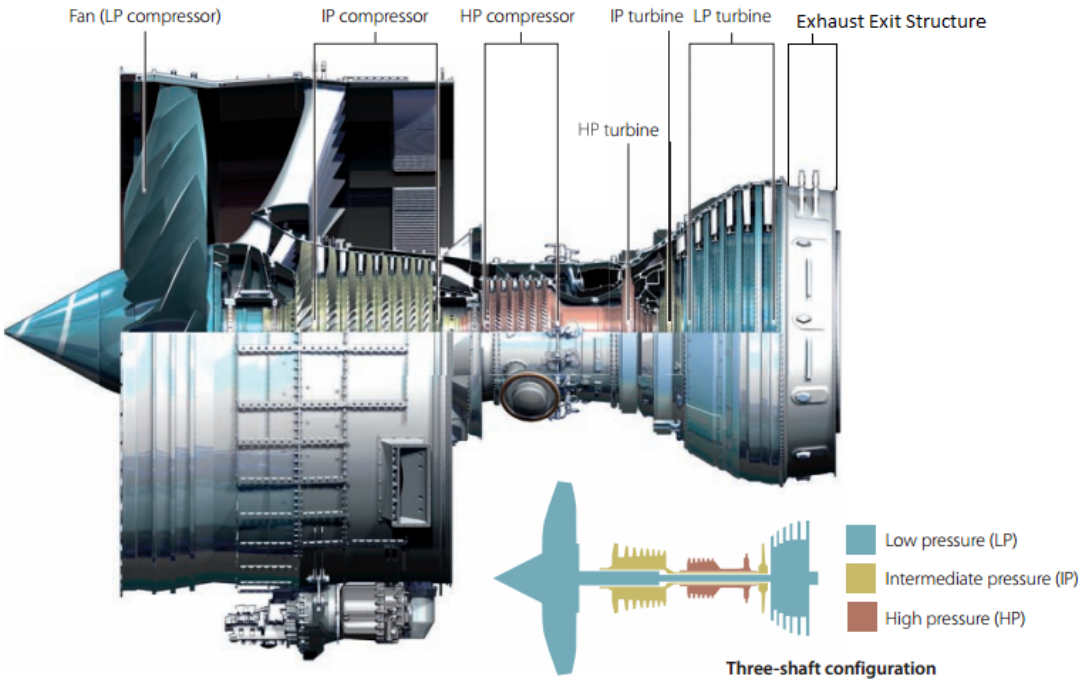

Figure 1.1: Turbofan jet engine

Figure 1.1 shows a jet engine with a Exit Engine Structure, which is located at the last part after the Low Pressure Turbine.

This makes up the Bryton Cycle, but for a jet engine, where is the field which is concerned at this thesis, it is used with some differences.
Because in gas turbines for the purpose of obtaining electric power one must maximize the net work that will result in the turbine moving the generator.

In a low-bypass jet engine, however, the minimum net work is required, which is what keeps up the compressor (and other aircraft systems). The rest of the usable internal energy of the gas is not extracted, but is maintained in the form of kinetic energy. The momentum with which the expelled gases are carried is what propels the air plane forward, according to Newton's third law. For high-bypass engines the main driving force is generated by the fan.

Figure 1.2 shows how the Brayton's cycle is applied for turbojet.

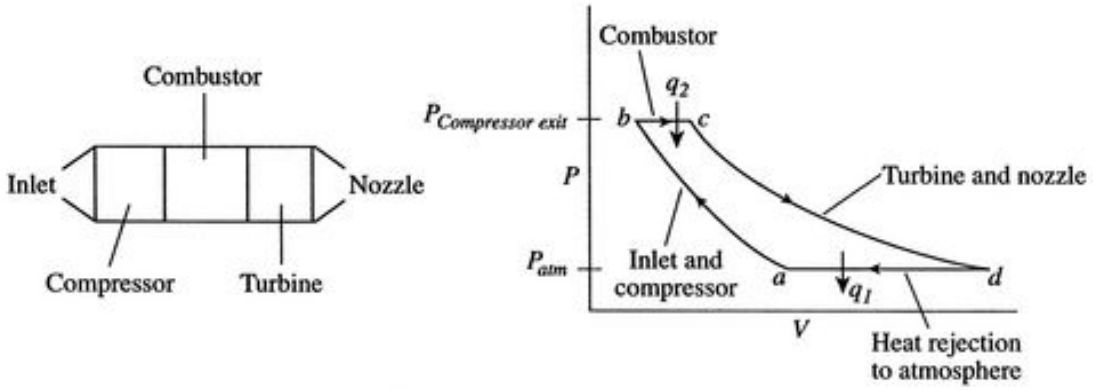

Figure 1.2: Brayton cycle

1.1.2 Outlet Guide Vanes (OGVs) description

The OGVs have both an aerodynamic and a structural function inside the gas turbine.
These vanes connects structurally the support for the rear connection of the motor, motor casing and the connection point of the aircraft. Meanwhile, the aerodynamic function of these vanes is to eliminate the tangential component of the air as these blades are the latest to the flow path before going into the nozzle. So it is very important to reduce aerodynamic losses at these crucial points in the turbine.

The most important areas of an OGV are the following , that are shown in Fig. 1.3.

A Leading edge.

B Trailing edge.

C Shroud side.

D Hub side.

E Suction side.

F Pressure side.

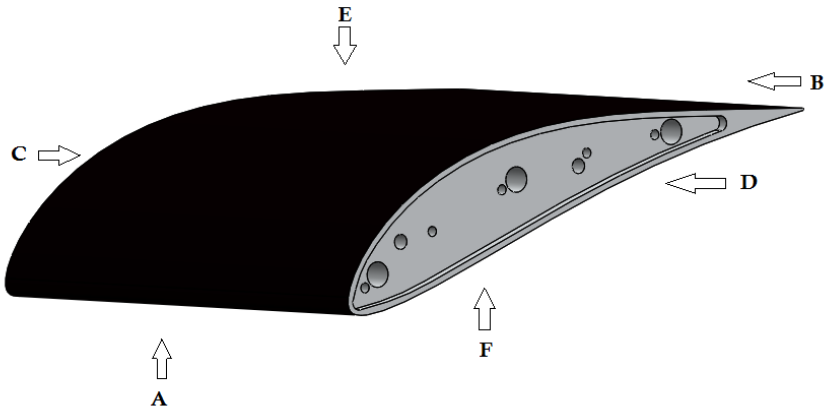

Figure 1.3: Areas of an OGV

Through the surface of the vane there is a distribution of pressures which is affected by the design of it. In order to study this distribution the pressure coefficient is used, which is a non-dimensional coefficient that describes the relative pressure through a flow field. This coefficient depends on the air foil shape, inlet velocity magnitude and inlet velocity relative angle.

At on-design conditions the pressure distribution coefficient is negative at the pressure side. The C_p is plotted "upside-down" with negative values (suction), higher on the plot because the upper surface uses to correspond to the upper line (see [1] and Fig. 1.4).

The OGV that is used consists of a 2D profile section which is extended in the span direction. One of them composed of an aluminium core and silicone shell to study the heat transfer, being able to insert some electrical heaters and a thermoresistor. The others vanes used in the linear cascade are made of plastic by using SLA (stereolithography) technique for the aero-measurements.

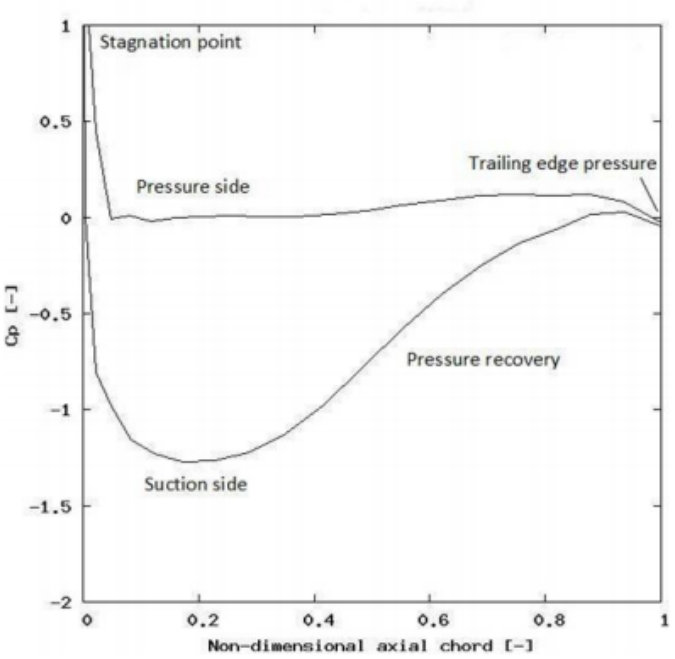

Figure 1.4: Pressure distribution on an airfoil.

1.1.3 The facility

The facility where the experiments were performed is located at Chalmers University of Technology and is a subsonic linear cascade rig. The rig was assembled in 2004, the test section has a cross section of 1200 x 240 mm^2 and with the power fan of 30 kW the maximum inlet wind speed achieved is 30 m/s, being able to run experiments at realistic Reynolds numbers.

Furthermore, it is possible to locate different kind of vanes to a Plexiglas wall, which allows use optical measurements. This test area is 1200 mm length, where can be located 4 vanes. To be able to test different designs, the angle of the inlet air flow can be changed from 0^o to 52^o. The rig is also equipped with an advanced suction system driven by two motors with 15 kW power to control the growth of the boundary layers on the side walls.

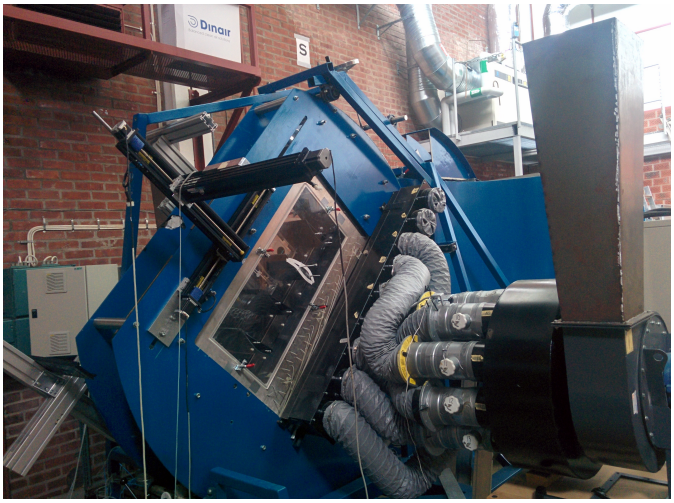

Figure 1.5: Chalmers' Subsonic Linear Cascade Rig

1.1.4 Theoretical Background

Heat Transfer

Heat transfer is the science that predicts the energy exchanged amongst two bodies with different temperature. Whenever there exists a temperature difference in a medium or between different media, heat transfer must occur. This science explains how the energy is exchanged and it can guess the velocity of this exchange at different conditions. This is different than the thermodynamics, because the last one studies systems which are in equilibrium or how to change one equilibrium system to another state of equilibrium, but not the rates.

Heat transfer mechanisms

The heat transfer is transferring energy as a result of a driving force, which is the temperature difference. The heat flow occurs when two different temperature bodies come into a thermal contact and the heat flow goes from the object with higher temperature to the lower temperature. There are three ways in which heat is transmitted, which depends on the nature of the system and the conditions under which it is located.

Conductivity

Conductivity is the molecular transport of heat, and is a consequence of the electronic migration between atoms in a rigid network or the transmission of the vibration energy between adjacent molecules in a solid, however in a fluid is the direct interaction between its molecules without a macroscopic fluid displacement. The energy level of the elemental particles is a temperature function, due when these particles move to a minor temperature regions, these particles cease their excess energy to other particles with less temperature as heat.

The heat flux by conduction is given by Fourier's law:

$$\mathbf{q} = k\nabla T \quad (W/m^2) \tag{1.1}$$

k is the material's thermal conductivity ($Wm^{-1}K^{-1}$), which is analogous to the Newtonian viscosity, which is a property of transport and is defined as the energy needed to heat one cubic meter of the material by one degree.

The conductivity of pure metals decreases with the temperature. However, for alloys depends on the composition. For liquids and gases the conductivity is increased by the temperature.

The minus sign indicates the physical fact that the heat flux goes from high to low temperature.

The differential equation for the heat conduction in Cartesian coordinates is.

$$\begin{aligned} &\frac{\partial}{\partial x}\left(k\frac{\partial T}{\partial x}\right) + \frac{\partial}{\partial y}\left(k\frac{\partial T}{\partial y}\right) + \frac{\partial}{\partial z}\left(k\frac{\partial T}{\partial z}\right) + q_0 = \rho Cp\frac{\partial T}{\partial t} \\ &T = T(x,y,z,t); \\ &q_0 = q_0(x,y,z,t) \end{aligned} \tag{1.2}$$

Where x,y,z are the spatial coordinates of the body to study, q_0 is the heat generated per volume (W/m^3) ρ is the density (kg/m^3) and Cp is the specific heat ($J/(K \cdot kg)$) For a unidirectional energy transport the last equation is simplified to:

$$k\frac{d^2T}{dx^2} = 0 \tag{1.3}$$

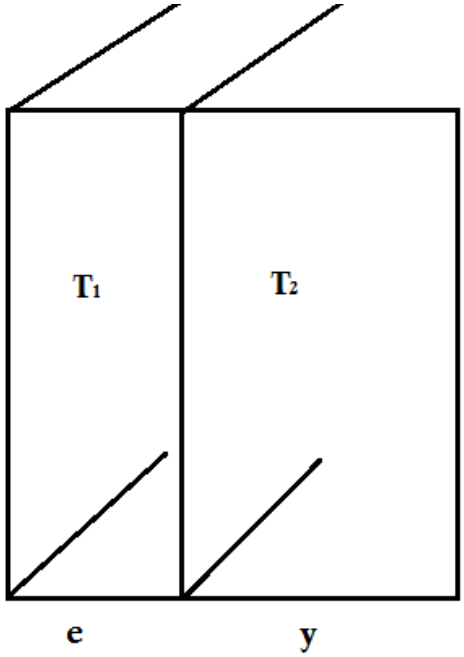

Figure 1.6: Conduction in a flat wall

When the equation 1.3 is integrated and with the following boundary conditions:

$$B.C.1: \quad y = 0; \quad T = T_1; \quad \frac{dT}{dy} = C_1; T = C_1 y + C_2$$

$$B.C.2: \quad y = e; \quad T = T_2; \quad T_1 = C_2$$
$$T_2 = C_1 \cdot e + C_2;\ T_2 = C_1 \cdot e + T_1$$
$$C_1 = C_1 \frac{T_2 - T_1}{e}$$

Therefore, the temperature it is:

$$T = \frac{T_2 - T_1}{e} y + T_1 \tag{1.4}$$

And the heat flux it is:

$$q = q_A \cdot A = -k \frac{dT}{dy} A = k \frac{T_1 - T_2}{e} A \tag{1.5}$$

In a flat wall with several materials is the same for each interface.

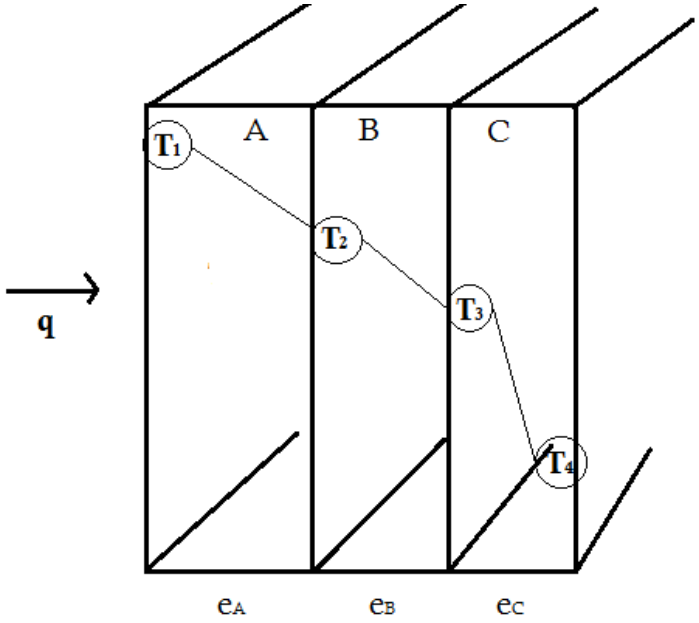

Figure 1.7: Conduction in a flat wall with several materials

$$q = \frac{T_1 - T_2}{\left(\frac{e}{kA}\right)_A} = \frac{T_2 - T_3}{\left(\frac{e}{kA}\right)_B} = \frac{T_3 - T_4}{\left(\frac{e}{kA}\right)_C} = \frac{T_1 - T_4}{\left(\frac{e}{kA}\right)_A + \left(\frac{e}{kA}\right)_B + \left(\frac{e}{kA}\right)_C} \tag{1.6}$$

Convection

Convection is the heat transfer among macroscopic movement of fluid particles. Convection is due to the movement of a fluid via a density gradient or mechanical energy. The heat transfer in this mechanism is due to conductivity and radiation when the moved material interact with its surrounds.

Boundary layer

The concept of boundary layer was introduced first by Prandtl in 1904. When a fluid moves next to a solid wall, the fluid particles in contact with the wall are adhered to its surface due to fluid viscosity. There is a zone where the fluid velocity is between zero and 0.99 $\cdot U_\infty$ (U_∞ is the velocity of the fluid at infinity, far from the solid). This zone is called boundary layer, it is dominated by viscosity and it creates the majority of drag.

In heat transfer aspects, it is considered that the majority of the heat transfer to and from a body also takes place within the boundary layer.
For this case the equation is.

$$q = kA\frac{T_{wall} - T_{inf}}{\delta}$$

As δ cannot be measured, it is combined with k, the result is h, the convection heat transfer coefficient which depends on the cp, μ, ρ, k, flux conditions and the geometry.

Radiation

Thermal radiation is energy emitted by matter that is at a non-zero temperature. Although we will focus on radiation from solid surfaces, emission may also occur from liquids and gases. Regardless of the form of the matter, the emission may be attributed to changes in the electron configurations of the constituent atoms or molecules. the energy of the radiation field is transported by electromagnetic waves (or alternatively, photons). While the transfer of energy by conduction or convection requires the presence of a material medium,radiation does not. In fact, radiation transfer occurs most efficiently in a vacuum.

To understand its importance; life as we know it depends on electromagnetic radiation from the Sun. This mechanism is the only way that propagates heat between this two bodies with different temperatures.

Corpuscle-wave theory Radiation can be explained by the corpuscle-wave theory, this theory considers separately the emission and reception of radiation.
The propagation of the radiation is done only in "chunks" of energy, quanta E, also called photons. The photon energy is defined by its frequency according to by Planck's law.

$$e = h \cdot \upsilon \tag{1.7}$$

In this equation h is the Planck's constant; $h = 6.62377 \cdot 10^{-34} J \cdot s$, and υ is the frequency, it is the number of oscillations per second. The wave length and the frequency are related with its velocity.

$$\lambda = \frac{c}{\upsilon} \tag{1.8}$$

Where c is the speed of light through the material. The speed of light in vacuum is c_0.

$$c_0 = 2.99776 \cdot 10^8 m/s^{-1}$$

Throughout other materials or fluids the velocity decreases, the ratio between this velocity is called refractive index, n.

$$n = {}^{c_0}/_{c} \tag{1.9}$$

Radiation is used to designate the energy transmission through space by electromagnetic waves. It includes the full range of energy, from radio waves, X-rays, γ and cosmic rays to visible light or even radio. The wave range which includes the thermal radiation is 0.1 to 100μm.

Radiation proprieties The electromagnetic waves moves through the space following straight lines. When a ray impacts in a body's surface, one part of this radiation is absorbed (absorptivity α), other part is reflected (reflectivity ρ), and other part is transmitted (transmissivity τ).

$$\alpha + \rho + \tau = 1 \tag{1.10}$$

There are two different kinds of reflectivity.

Diffuse reflection occurs when an incidental ray of light strikes a surface and the light is scattered. In perfect or ideal diffuse reflection, all the light is perfectly distributed around the point it strikes the diffusion surface in a hemisphere of illumination. Specular reflection occurs when an incidental ray of light strikes a surface and is reflected at the same angle of incidence (both taken perpendicular to the plane at the incidence point).

Black body To explain how the radiation works, an ideal surface is introduced, the "Black body". It has the following surface properties.

- A black body always absorbs the radiation, at any wavelength or direction.
- The black body radiates more energy than any real surface.

- The radiation emitted by a black body, it is function of the temperature and the wavelength, but not of the direction. A black body has diffuse emissivity.

Therefore, it ideally absorbs and emits thermal radiation. And it is used to model real systems.

Planck's, Wien's and Stefan-Boltzmann's laws

Radiant energy distribution. Planck's law. Any body at a particular temperature emits radiation in a wide wavelength range but in the laboratory is possible to obtain a monochromatic light, it is radiation with a certain wavelength. Planck determinates that the monochromatic energy in a black body per surface, time and wavelength is a function of the wavelength and the temperature.

$$I_{\lambda,T}(\lambda,T) = \frac{2\pi h \cdot c_0^2 \cdot \lambda^{-5}}{\left(e^{\frac{h \cdot c_0^2}{k \cdot \lambda \cdot T}} - 1\right)} = \frac{C_1 \cdot \lambda^{-5}}{\left(e^{\frac{C_2}{\lambda \cdot T}} - 1\right)} \tag{1.11}$$

- h is the Planck's constant. $(6.6256 \cdot 10^{-34}\, J \cdot s)$
- c_0 is the light velocity in the vacuum. $(2.998 \cdot 10^{8}\, m/s)$
- k is the Boltzmann's constant.$(1.3806488 \cdot 10^{-23}\, J/K)$
- C_1 is the first radiation constant. $(3.7415 \cdot 10^{-16}\, W \cdot m^2)$
- C_2 is the second radiation constant. $(0.01439\, m \cdot K)$
- T is the body's absolute temperature.(K)
- $I_{T\lambda}$ is the monochromatic emissive power of the black body.(W/m^2)

The spectral region where the radiation is focused depends on the temperature. The higher the temperatures the shorter the wavelength.

Wien's law Equation 1.11 shows that for each temperature there is a wavelength where the emissive power is the highest. Equation 1.12 shows the relation between the λ_{max} and temperature.

$$\lambda_{E_{N\lambda_{max}}} = \frac{2.878 \cdot 10^{-3}}{T} \tag{1.12}$$

Where the wavelength that provides maximum emissivity is inversely proportional to the absolute temperature. This number $(2.878 \cdot 10^{-3} m \cdot K)$ is called the third radiation constant.

Stefan-Boltzmann law. The total emissive power is a contribution of all wavelengths emitted by the body, it is therefore the sum of all monochromatic radiations.

$$E_N = \int_0^\infty \frac{C_1 \cdot \lambda^{-5}}{\left(e^{\frac{C_2}{\lambda \cdot T}} - 1\right)} \cdot d\lambda \tag{1.13}$$

The total emissive power of a black body is shown in Eq. 1.14.

$$E_N = \sigma \cdot T^4 \tag{1.14}$$

Where σ is the Boltzmann's constant, which is $5.67 \cdot 10^{-8}\,(W\,m^{-2}\,K^{-4})$. For non-black bodies the concept of surface emissivity is used, which is the relation between the total emissive power for a non-black body (E) and a total emissive power for a black body (E_N) at the same temperature.

$$\varepsilon = \frac{E}{E_N}; \qquad E = \varepsilon \cdot \sigma \cdot T^4 \tag{1.15}$$

Kirchhoff's laws

First Kirchhoff's law. When is achieved the thermal equilibrium the relations between the emissive power and the absorptivity of all bodies is constant and it is function of the equilibrium temperature.

$$E_N = \frac{E_1}{\alpha_1} = \frac{E_2}{\alpha_2} = ... = \frac{E_n}{\alpha_n} = f(T) \tag{1.16}$$

Where the subscript number is the name of the non-black body involved at thermal equilibrium.

Second Kirchhoff's law. From the definition of emissivity, it can be formulated in a thermal equilibrium:

$$E = \alpha \cdot E_N \qquad and \qquad E = \varepsilon \cdot E_N$$

So in a thermal equilibrium, the emissivity and absorptivity of all bodies are the same value.

Theoretical model for heat transfer measurement technique

All this mechanisms can happen at the same time. The theoretical model for our experimental set up which explain how they occur can be seen in Fig. 1.8.

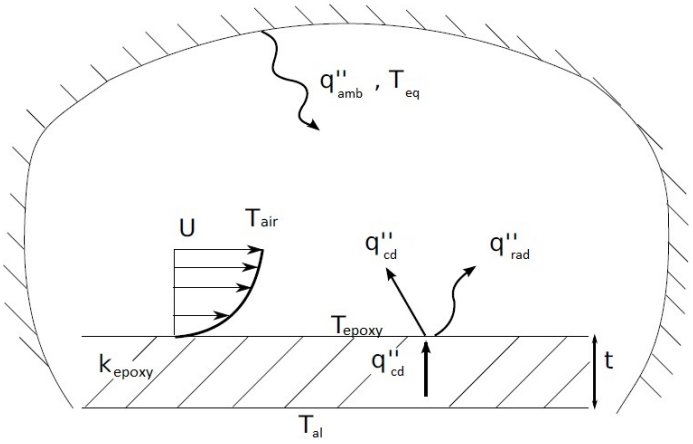

Figure 1.8: Model for the HTC experiment

The set up is composed by a aluminium sheet with heaters and an epoxy layer, from the aluminium core the heat fluxes goes through the epoxy layer, with a t thickness, to the outside. These heat fluxes can be calculated following these equations:

- Conduction heat flux

$$q''_{cd} = k \cdot \frac{(T_{al} - T_{epoxy})}{t} \tag{1.17}$$

- Convection heat flux

$$q''_{cv} = h \cdot \frac{(T_{epoxy} - T_{air})}{t} \tag{1.18}$$

- Net radiation heat flux

$$q''_{rad} \simeq \varepsilon \cdot \sigma(T^4_{epoxy} - T^4_{eq}) \tag{1.19}$$

To calculate the HTC or h all the parameters required are known, as the temperatures at each point, the temperature of the aluminium-epoxy interface T_al, the epoxy temperature T_epoxy, the ambient temperature or the thermal conductivity of the epoxy. In this experiment the ϵ used is the thermal emissivity of the surface of the epoxy, which has been painted to convert it in a nearly black body, using Nextel Vetel-Coating 811-21 from Mankiewicz Gebr. & R Co. This thermal emissivity is constant at the temperatures that this end-wall works.($\epsilon = 0.973$)

As it can be seen in the figure, the convection heat flux and the radiation heat flux comes from the conductivity heat flux. Therefore, a energy balance:

$$q''_{cd} = q''_{cv} + q''_{rad} \tag{1.20}$$

Finally to calculate the HTC, can be calculated by this equation:

$$HTC = \frac{k \cdot \frac{(T_{al} - T_{epoxy})}{t} - \epsilon \cdot \sigma \left(T^4_{epoxy} - T^4_{eq}\right)}{T_{plexy} - T_{air}} \tag{1.21}$$

FEM (How it works: SolidWorks Simulation)

Modern design is conducted using Computer-Aided Design (CAD), therefore a CAD model is the starting point for the analysis. In this project, the program that has been used for CAD is SolidWorks.

SolidWorks Simulations uses Finite Elements Method (FEM), which is a numerical analysis method, for calculating temperature distributions.

It is used for solving problems in many engineering disciplines, this numerical technique is used for solving field problems described by a set of partial differential equations.
FEA has been used as a design tool. This is changing the design in repetitive cycles of design, prototype and test.

Once the part or assembly is designed in SolidWorks, FEA has the information of the material properties, defined constraints and the geometry. At the meshing part, FEA splits geometry into small and simply shaped entities called finite elements, which are finite because are not infinitesimally small but smaller than all the model size. Then FEA works with finite elements, and the solver approximates the solution by assembling the solutions for individual elements. [2]

Sometimes in FEA, it is necessary to clean up the geometry, which is performed simplifying the geometry. For two reasons is required. Firstly because the geometry has to be able to be meshed, because sometimes little details are really difficult to mesh, and secondly because it will require less iterations to obtain a converged solution.

Errors in FEA Formulation of a mathematical model introduces modelling errors, discretization of the mathematical model introduces discretization error, and solving introduces solution errors. Of these three kind of errors, just discretization errors are specific to FEA. Modelling errors affecting the mathematical model are introduced previous to FEA is utilized and can only be controlled by using correct modelling techniques. [3]

Thermal simulation using FEA Each degree of freedom of a node in a finite element mesh is an unknown. On thermal analysis they represent temperatures. After found the temperatures, the thermal analysis finds the temperature gradients, and heat flow.

In these simulations only heat transfer by conduction is modelled directly, convection and radiation are modelled as boundary conditions. This is done by defining the convection and/or radiation coefficients to faces that participates in the heat exchange. No convection coefficients defined for those surfaces means no heat flows across them.

Flow measurements

As it is only required for our study be known the fluid velocity (both magnitude and direction) within the vane path, is only measured the total pressure and the static pressure. Once this data is acquired, the fluid field velocity is calculated. This is possible with a Pitot tube that was invented by Henri Pitot in 1732.

A Pitot tube or similar velocity-measuring device consists of a cylindrical tube with an open end pointed upstream, used for measuring total pressure. Another opening is located in its side wall to measure the static pressure. The difference between the impact pressure and the static pressure is a function of the velocity and the density of flow past the tube.

Then Bernoulli's equation is applied to calculate the fluid velocity. The Bernoulli's principle is applied to various types of fluid flow and is derived from the principle of conservation of mechanical energy. This is, in a steady flow, the sum of all forms of mechanical energy in a fluid along a streamline is identical at all points. This involves that the sum of kinetic energy and potential energy remain constant. Hence an increase in the speed of the fluid occurs proportionately with an increase in both its dynamic pressure and kinetic energy, and a decrease in its static pressure and potential energy. This is:

$$P_t - P_s = \frac{1}{2} \cdot \rho v^2 \tag{1.22}$$

Where P_t is the total pressure, and P_s the static pressure, both measured by the Pitot tube. While ρ is the air density, which is known by measuring the temperature of the air flow and using the ideal gas equation assuming atmospheric pressure.

Equation 23 shows how it is calculated the speed on a certain position.

$$v = \sqrt{\frac{(P_t - P_s) \cdot 2}{\rho}} \tag{1.23}$$

In regions where the dynamic pressure is negative, the velocity is undefined. This points out that there might be a recirculated areas.

2

End-wall design

2.1 Introduction

For the heat transfer experiments is necessary an instrumented window. To calculate the heat transfer is necessary to measure temperatures on both sides of the epoxy layer. So it is included some thermoresistors to measure the temperature inside the end-wall, and an IR-camera to measure the temperature at the surface. The material in contact with the air has a low thermal conductivity in order to obtain a large temperature gradient between the layers and to be able to measure the temperatures at each layer accurately.

The design has to take into account the geometry of the end-wall and configuration of the components to guarantee that the theoretical model for the heat transfer measurement can be used.

2.2 Design process

The main objective of the design of this end-wall is to provide a long term instrumented window to Chalmers. Therefore, this device has to be accurate at its measurements so a uniform temperature distribution is needed. It is also crucial to avoid air gaps inside the model. The air inside the piece or between layers can affect the thermal distribution due to the insulating properties of the air. Another important issue to take care of is how to measure the temperature inside the piece to calculate the HTC.

To make sure that the final piece satisfies these requirements, it has been studied in each case what was the best solution and adapting the design to get it.

2.2.1 First design

The very first design was one piece of aluminium, where inside it could be found cylindrical heaters, avoiding any superficial effect as mentioned above, because air gaps could appear with flat heaters between two aluminium heaters. On this sheet was attached a thin Plexyglass sheet by nylon screws to the aluminium surface. Finally, a framework consisting of four nylon pieces, them would hold all the parts including the insulation. It is remarkable that it had some gaps into the design, which have been filled by air.

To avoid this gaps and make sure that is a compact design, the framework was rebuilt in such a way that it fills this holes.(see [5]).

2.2.2 Heaters optimization

One point really important at the design has been the uniformity of the temperatures, to be able to map the temperature gradient among the surface with the thermoresistors.

For that, the prototype was reduced to its quarter due to its symmetry to be able to study it with more details. It has also been studied the possibility that one heater is broken and it is not working, and difference heat power for each heater as a result of its fabrication ($\pm 10\%$)

The heater distribution that has been tried to study is 16 heaters, 24 heaters and 30 heaters. There were distributed two at each row due its dimensions. The heater characteristics are: 10 mm x 100 mm, 120 V, 400 W

Figure 2.1 shows the parts that has been analysed. The X axis and the Y axis are the parametric distance of the reduced piece, 0 is the outer part of the piece and 1 it is the centre of the instrumented window.

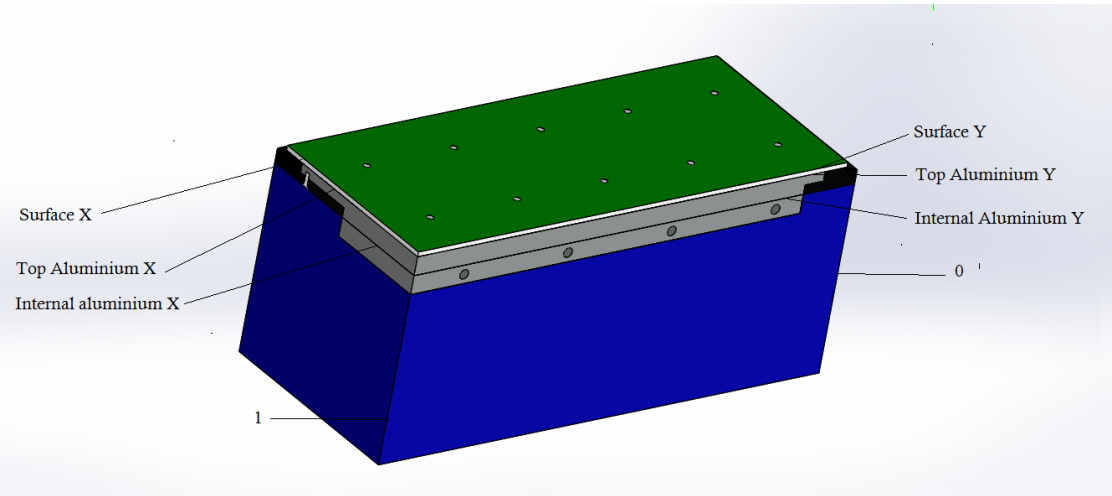

Figure 2.1: Analysed parts at the prototype for the heaters optimization.

During the SolidWorks simulations it could be seen the influence of the screws at the surface.

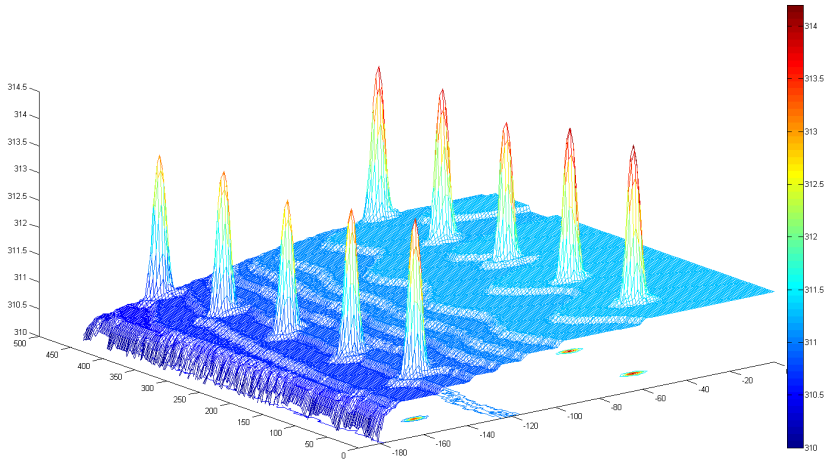

Figure 2.2: Temperature distribution at the surface. Design with Nylon screws.

The nylon screws that held them on to the aluminium could affect locally the temperature distribution. It is because it has been decided to change the Plexyglas layer for an epoxy layer. This epoxy has the lowest viscosity achievable to avoid air bubbles inside it.

This epoxy layer will fill the gap from the aluminium surface until the nylon frame. Once cured it will be attached to the aluminium so it will not be necessary any sort of screws. To make sure that the liquid epoxy does not penetrate through gaps between different frame components, the framework is changed to a single piece of nylon.

Detailed results for thirty heaters.

The simulation obtained with 30 heaters is less uniform than expected as can be seen at Fig. 2.3, 2.4 and 2.5.

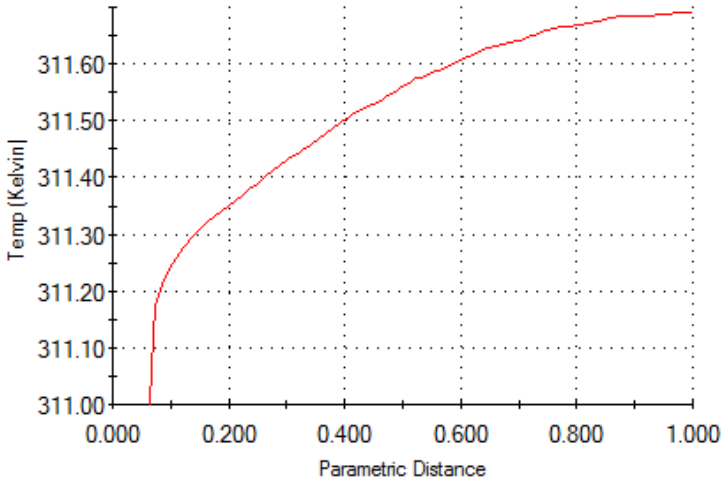

Figure 2.3: Temperature distribution along the surface epoxy. 30 heaters.

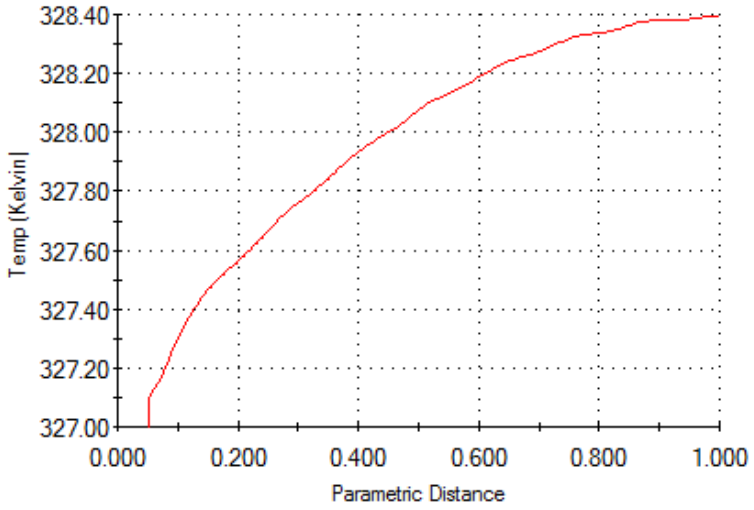

Figure 2.4: Temperature distribution along the top surface of aluminium plate. 30 Heaters.

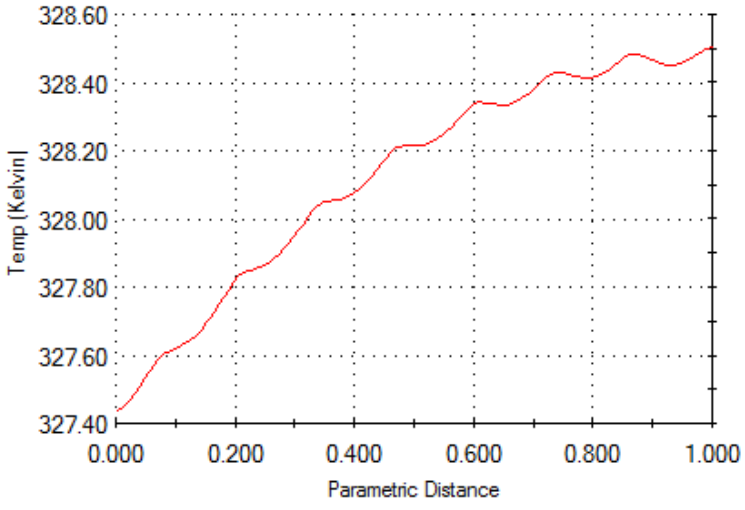

Figure 2.5: Temperature distribution along the internal aluminium. 30 Heaters.

Detailed results for sixteen Heaters.

With this set up the simulation is a little bit different as it can be seen at the Fig. 2.6, Fig. 2.7 and Fig. 2.8.

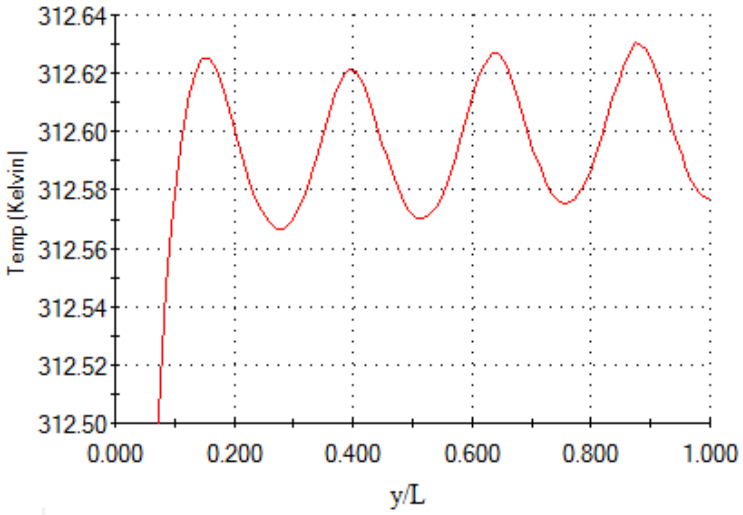

Figure 2.6: Temperature distribution along the surface epoxy. 16 heaters.

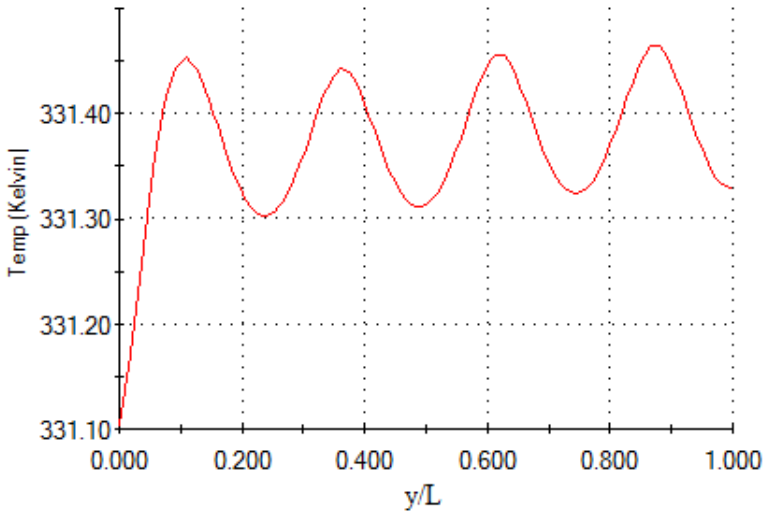

Figure 2.7: Temperature distribution along the top surface of aluminium plate. 16 Heaters.

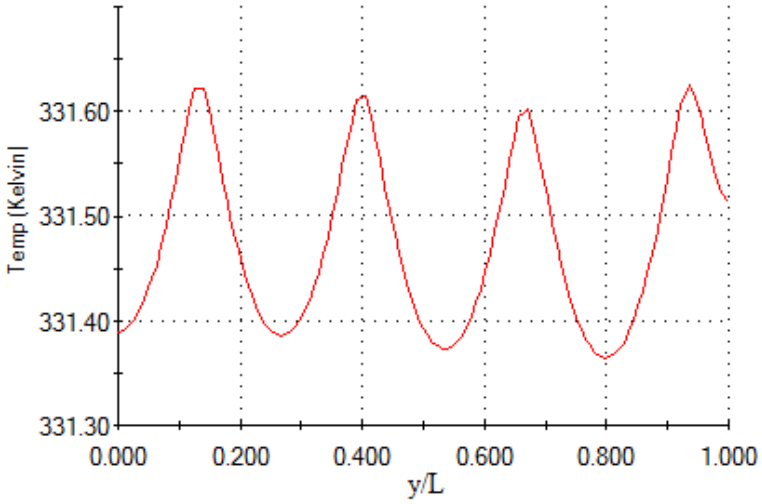

Figure 2.8: Temperature distribution along the internal aluminium. 16 Heaters.

Heat Optimization Conclusion As can be seen, the more heaters used, the more uniform the curve from the centre to the sides. But there are bigger differences between both extremes. However, a sinusoidal curve is obtained at the 16 heater distribution, but its amplitude is almost less 0.1 ºC, which is acceptable for this case.

In addition, non-uniform heat flux and heater switched off cases showed the same differences. This can be seen in the Appendix A1. Therefore, 16 heaters distribution has been chosen for this design, because it is needed less heaters and machining for the holes, being this design cheaper and being possible to obtain a uniformity temperature of 0.1 °C. The main outcome from this study can be summarized with the sentence "less is more".

2.2.3 Thermoresistor optimization

To measure the HTC with the instrumented window, temperatures of the Epoxy surface in contact with the air flow and the temperature of the aluminium-epoxy surface interface are needed. It is not possible to use an IR-camera to measure the surface temperature of the aluminium-epoxy surface interface. Therefore, it has been decided to use thermoresistors in order to measure different points in the aluminium and use an interpolation polynomial to calculate the temperature throughout the surface.

The accuracy of the interpolation depends on the distribution and number of the thermoresistors, which depends on the system response and the order of the interpolation polynomial used.

This optimization has been performed with a SolidWork's simulation, because it allows simulation of different scenarios (HTC distribution) for different thermoresistor patterns. Once the simulation is done, the data is exported to Matlab where the thermoresistors points are interpolated. The interpolated data is compared with the simulation.

This interpolation has been performed creating a Matlab script which imports the Solidworks simulation data to Matlab, that is, all the aluminium-epoxy surface interface and the thermoresistor points data (which consists of the data of one node from the same location as the thermoresistor would have).Afterwards, it is inserted which polynomial degree the user analyses on each axis.

This analysis has attempted three different polynomial grades for the least square interpolation: $\{x^3,y^3\}$, $\{x^3,y^2\}$, $\{x^2,y^2\}$, $\{x^2,y^3\}$. Obtaining better results with $\{x^2,y^2\}$.
Then the function used is *mldivide* or \ which solves systems of linear equations $A \cdot x = B$, where A is a rectangular m-by-n matrix, this matrix is the coordinates of the plane that is studied multiplied by the chosen polynomial, and B is the matrix with m rows with the temperatures of those coordinates. Then A\ B returns a least-squares solution to the system of equations A*X=B. [4]

$$A_{(m+1)x(n+1),c} = \begin{pmatrix} x_1^m \cdot y_1^n & x_1^m \cdot y_1^{n-1} & \cdots & x_1^m \cdot y_1^0 & x_1^{m-1} \cdot y_1^n & x_1^{m-1} \cdot y_1^{n-1} & \cdots & x_1^0 \cdot y_1^0 \\ x_2^m \cdot y_2^n & x_2^m \cdot y_2^{n-1} & \cdots & x_2^m \cdot y_2^0 & x_2^{m-1} \cdot y_2^n & x_2^{m-1} \cdot y_2^{n-1} & \cdots & x_2^0 \cdot y_2^0 \\ \vdots & \vdots & \ddots & \vdots & \vdots & \vdots & \ddots & \vdots \\ x_c^m \cdot y_c^n & x_c^m \cdot y_c^{n-1} & \cdots & x_c^m \cdot y_1^0 & x_c^{m-1} \cdot y_2^n & x_c^{m-1} \cdot y_c^{n-1} & \cdots & x_c^0 \cdot y_c^0 \end{pmatrix} \tag{2.1}$$

Where m is the degree at the x axis, n is the degree at y axis and c is the number of points with different coordinates x and y.

$$B_c = \begin{pmatrix} T_1 \\ T_2 \\ \vdots \\ T_c \end{pmatrix} \tag{2.2}$$

Equation 2.2 is a vector of the temperatures measured at the coordinates c.
The matrix X represents the coefficients for the polynomial.

For the optimization several patterns have been tried with a uniform HTC on the epoxy surface. The best three patterns were also checked on a random HTC surface and with a realistic HTC obtained by Rojo [5] experimentally.

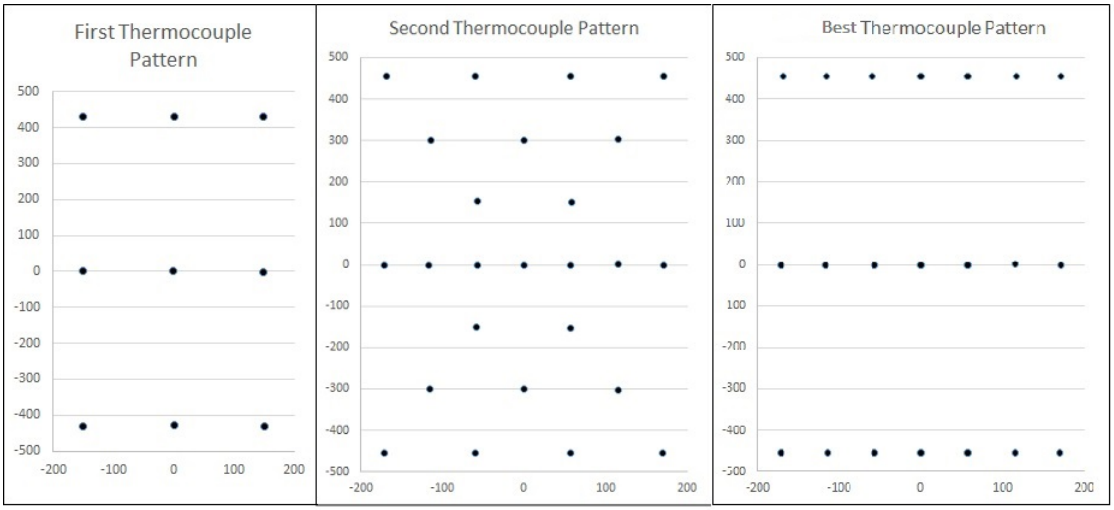

Figure 2.9: Different thermoresistor distribution.

Uniform convection heat transfer coefficient

For the first case, the convection coefficient at the epoxy surface is 60 $W/m \cdot K$, the same as in the heater distribution optimization. Once the thermal load is defined, the simulation data is imported to Matlab. The temperature where the thermoresistors are virtually located at the different patterns are also recollected. The results of this case with the best pattern and the best polynomial grade are shown in the Fig. 2.10, 2.11, 2.12 and 2.13.

Figure 2.10 shows the simulated temperature distribution throughout the aluminium-epoxy surface. This is the temperature that has to be known to be able to calculate the HTC. The other temperature is measured using the IR-camera.

Figure 2.11 shows the surface created by the interpolation polynomial calculated with the 21 points. The shape of the surface calculated with 21 points and the real one using thousands of points (between 15000 and 50000 nodes) as can be seen in Fig. 2.12 is almost the same.

Finally the error between the real data and the data interpolated is plotted at Fig. 2.13 in order to visualize the error distribution. The maximum differences are situated just at the ends of the piece, which are not relevant for this study because in those areas is not measured the heat transfer coefficient.

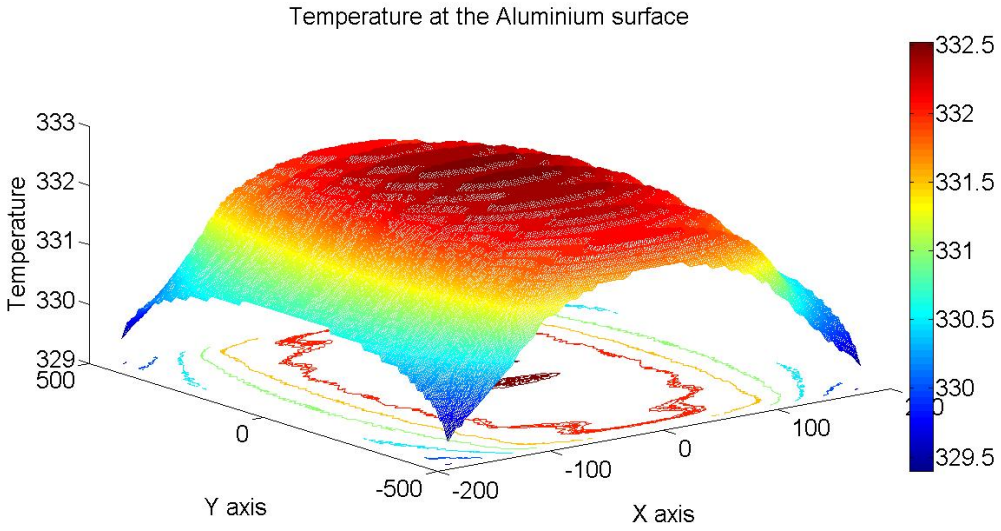

Figure 2.10: Simulation data with uniform convective coefficient.

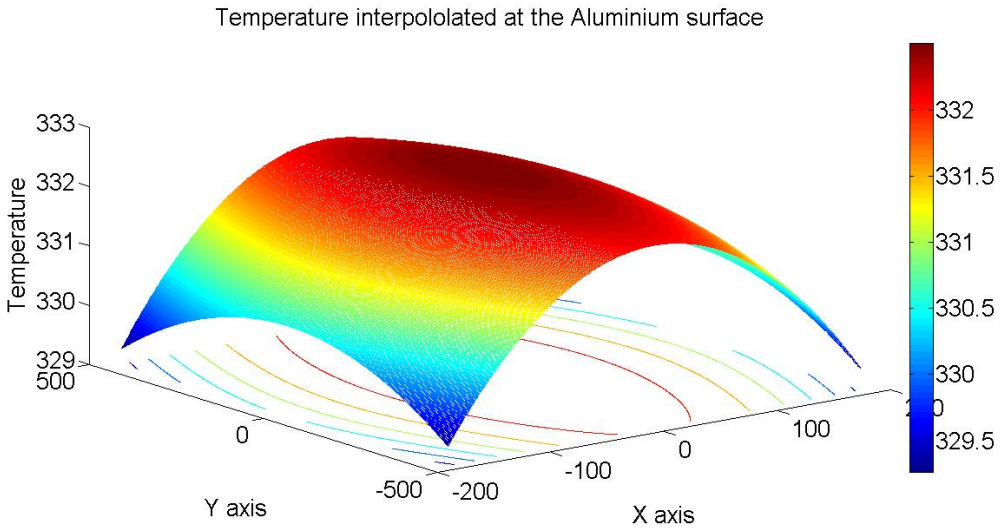

Figure 2.11: Calculated data using the interpolation with uniform convective coefficient.

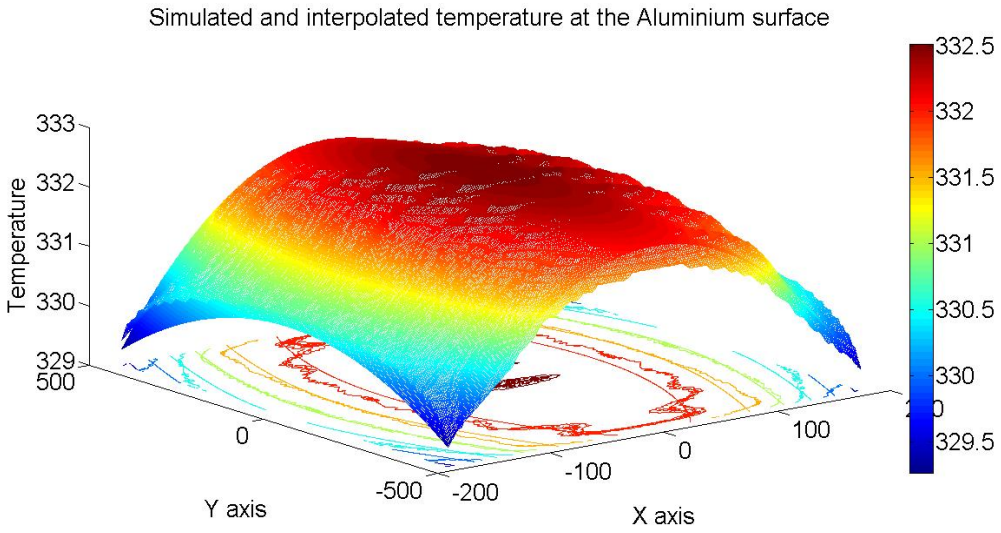

Figure 2.12: Simulation data and calculated data with uniform convective coefficient.

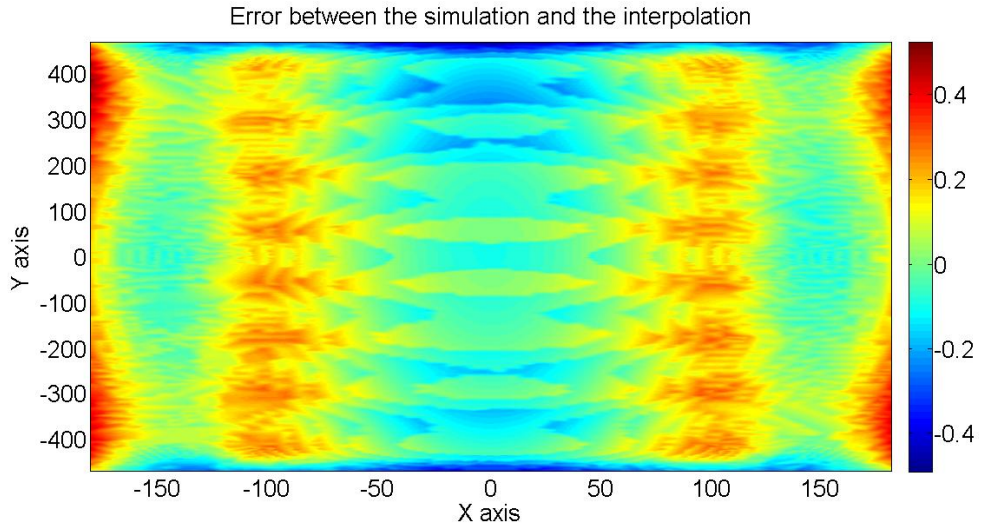

Figure 2.13: Error betweem simulation data and calculated data with uniform convective coefficient.

Such results are satisfactory, because the mean error is 0.03°C, the absolute mean error 0.10°C, this value is small, if we consider that an error of 0.10 or 0.20 results in 0.01% error of HTC. Furthermore, the maximum error is 0.52°C and the minimum error −0.50°C which are situated around the edges of the plate. The standard deviation of 0.13°C indicates a reliable method to calculate the temperatures throughout this surface.

Random convection coefficients

One study has been carried out with random convection coefficients to verify this method with such large temperature differences at the surface. These boundary conditions are more extreme than the the expected HTC values from the experiments. The coefficients at the various parts of the plate are shown in Fig. 2.14.

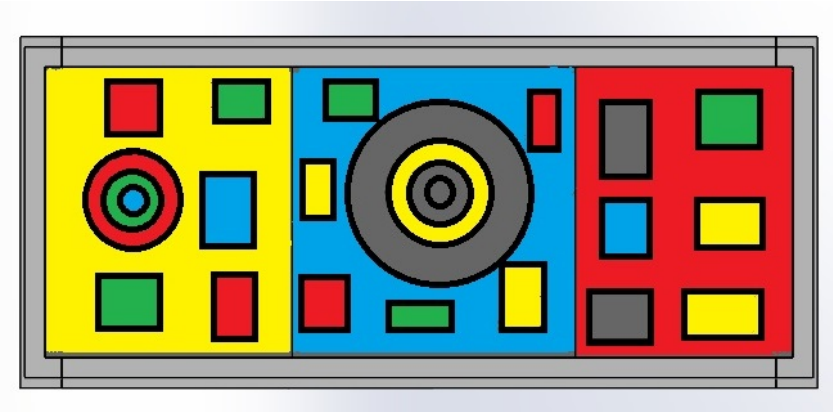

Figure 2.14: Mapping of the random convection coefficients.

Fig. 2.14 represents the different convection heat transfer coefficients applied in this case. At the blue zone, a convection coefficient of $120\,W/m^2 \cdot K$ is defined, at the red zone the value is $80\,W/m^2 \cdot K$, at the green zone the value defined is $60\,W/m^2 \cdot K$, at the grey zone is $40\,W/m^2 \cdot K$ and at the yellow zone is $20\,W/m^2 \cdot K$. Therefore, the surface obtained does not have a uniform temperature.
The epoxy surface and the aluminium surface with the different temperatures can be seen in Fig.2.15.

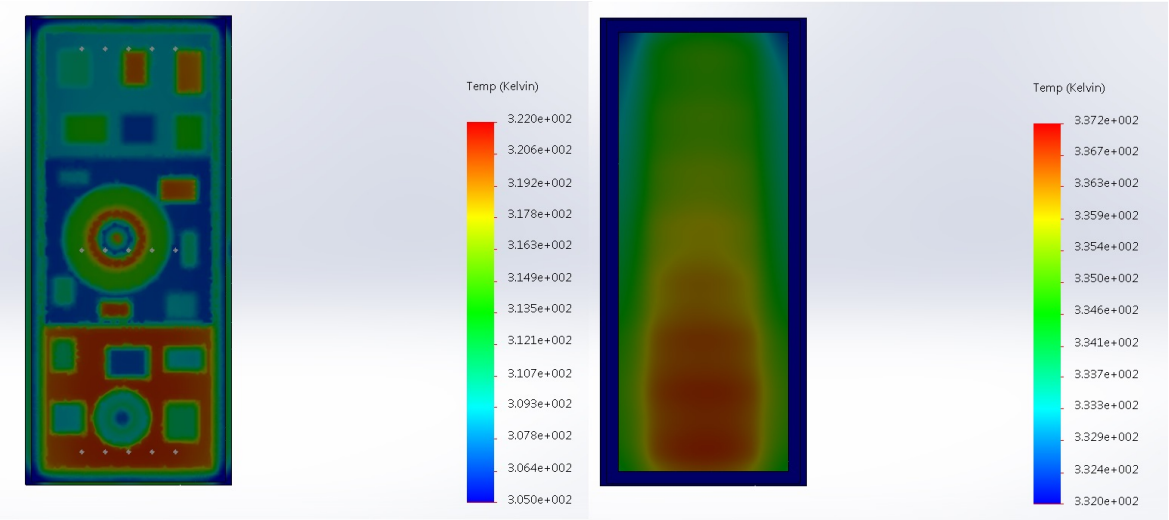

Figure 2.15: Left: Temperature thoughout the epoxy layer. Right: Temperature throughout the aluminium layer

Figures 2.15, 2.16, 2.17 and 2.18 show the simulation and analysed data.

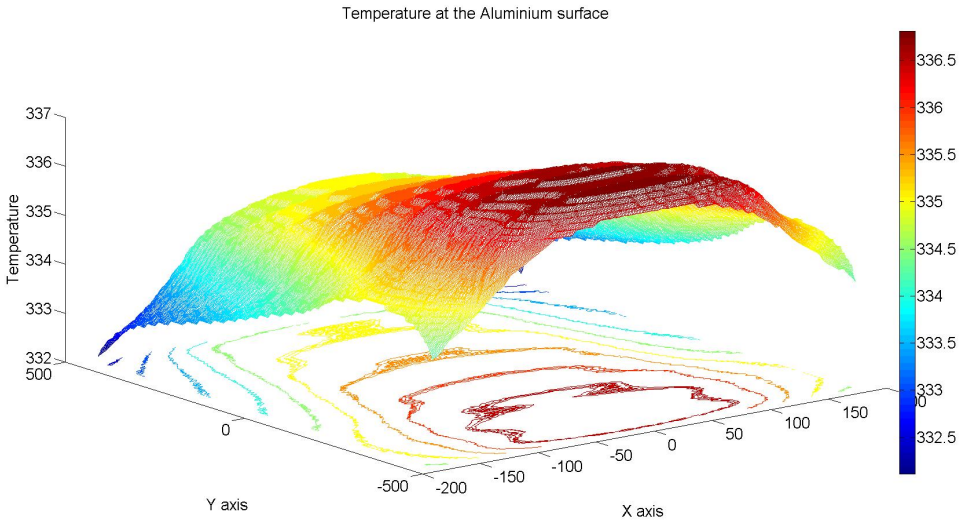

Figure 2.16: Simulation data with random convective coefficients.

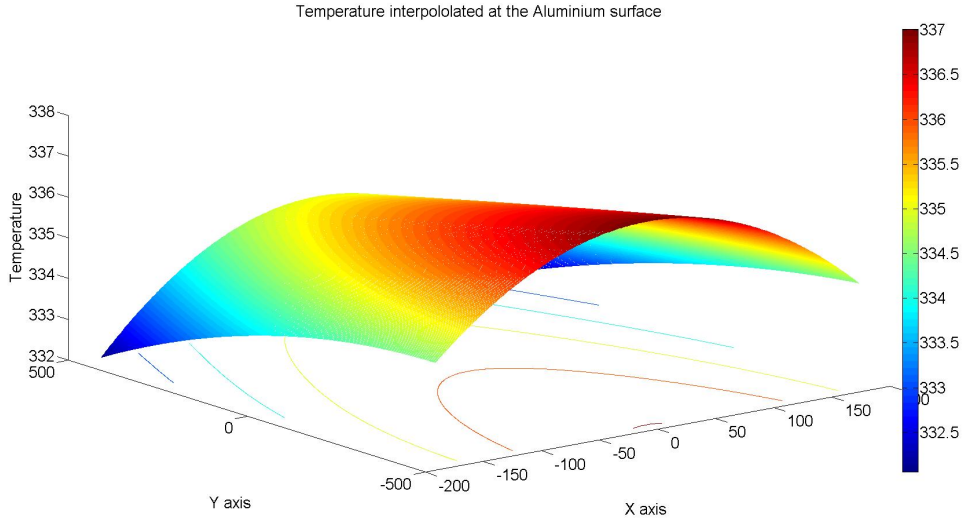

Figure 2.17: Calculated data based on the signal from simulated temperature sensors with random convective coefficients.

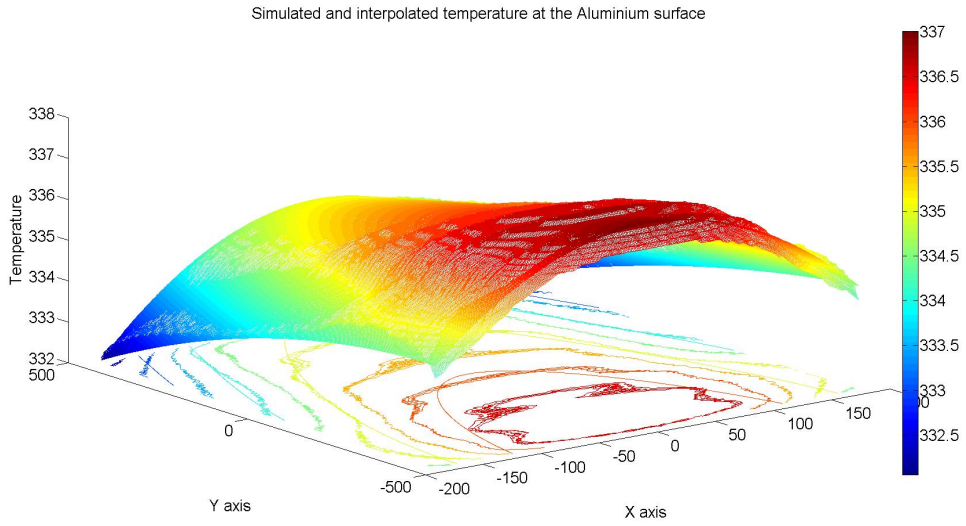

Figure 2.18: Simulation data and calculated temperature with random convective coefficients.

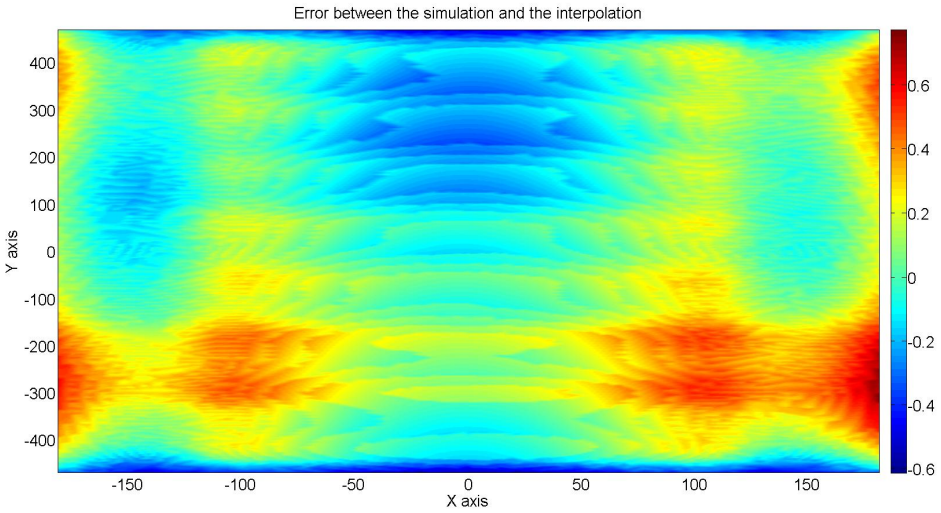

Figure 2.19: Error between simulation data and calculated data based on the signal from simulated temperature sensors with random convective coefficients.

Fig. 2.16 shows that the temperature is not symmetrical in this set up, but there is a gradual temperature change without any discontinuity through of the epoxy surface (see 2.18). This is because of the low thermal conductivity of the epoxy and the width of the aluminium sheet. The temperature distribution from simulated temperature sensors method that has been used for this case is showed in Fig. 2.17

Figure 2.17 shows the epoxy-aluminium surface interface temperature calculated with the data from the 21 points, which shows little difference from the simulated data.

The difference between this data is the error, which is shown in Fig 2.19 to indicate the difference in temperature.

Even though the conditions of this experiment are extreme, the results are satisfactory, because the mean error is 0.05°C and the absolute mean error 0.15°C. This value is small and similar to the previous scenario. Furthermore, the maximum error is 0.78°C and the minimum error -0.61°C situated around the edges of the plate or in small areas. The standard deviation of 0.19°C means that the errors are higher than in the previous study but it remain low.

2.3 The end-wall

The end-wall is composed of several parts: A 5 *mm* epoxy layer, which helps to obtain the HTC due its low thermal conductivity because creates a significant temperature difference on both faces; a nylon frame, which holds the end-wall in place; an aluminium sheet that due its high thermal conductivity and width, is needed to create a uniform temperature field under the epoxy layer; sixteen cylindrical heaters to heat up the end-wall; twenty-one thermoresistors to map the temperature inside the end-wall; twenty-four M6x40mm nylon screws to hold the frame to the aluminium plate; four nylon pieces to fix the handle to the aluminium plate.

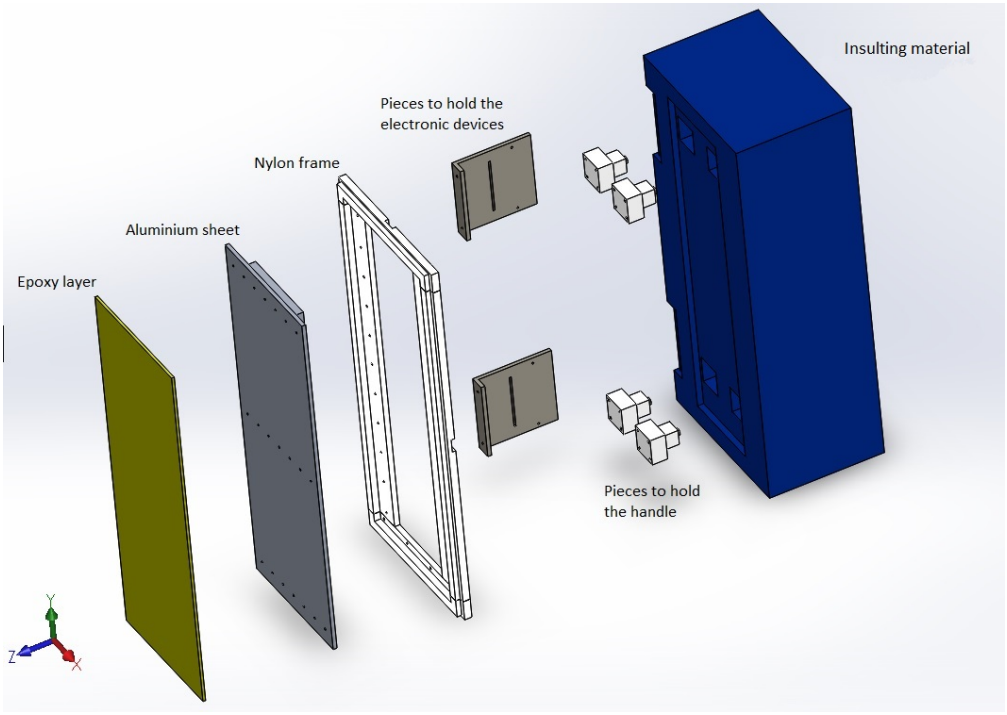

Figure 2.20: Exploded view

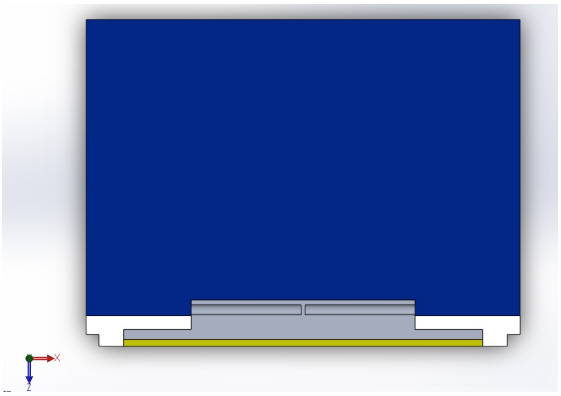

Figure 2.21: Cross section view

The drawings of the window can be found in the Appendix A.2.

3

Flow measurements

The flow measurements are performed in order to study the air flow field and how it can influence the HTC. Another reason to carry out this analysis is because it is of importance for CFD validation purposes.
To be able to know how the flow behaves at the linear cascade, it is necessary to know the air parameters at each moment. Therefore the temperature, density, pressure drop, viscosity and the atmospheric pressure have been measured.

The studies have been performed for three different vane relative positions, two off-design and one on-design position. The inlet relative angle for the on-design case is 25°, for the two off-design cases it has been used a 40° and -25°. Each case has been studied for a two different Reynolds numbers, 300000 and 450000.

The measurements are made using a Pitot tube, which measures the total pressure and static pressure with a sample time of two seconds. The tube with the aid of traversing system and software is guided through a set and measured at each grid point. The grid decreases in size near the end-wall and near the vane. The distance on the y axis of the mesh increases geometrically with a ratio of 1.2 until it reaches the middle of the path, then the distance between points decreases with the same coefficient until the mesh reaches the next vane. On the z axis the mesh increases following the same coefficient until it reaches the middle of the vane. It is possible to carefully measure the boundary layer with this kind of mesh, which is the most variable and interesting area. Saving time measuring the free flow.

The grid can be seen in the Fig. 3.1, where are the parametric distances at the y and z axis of the path.

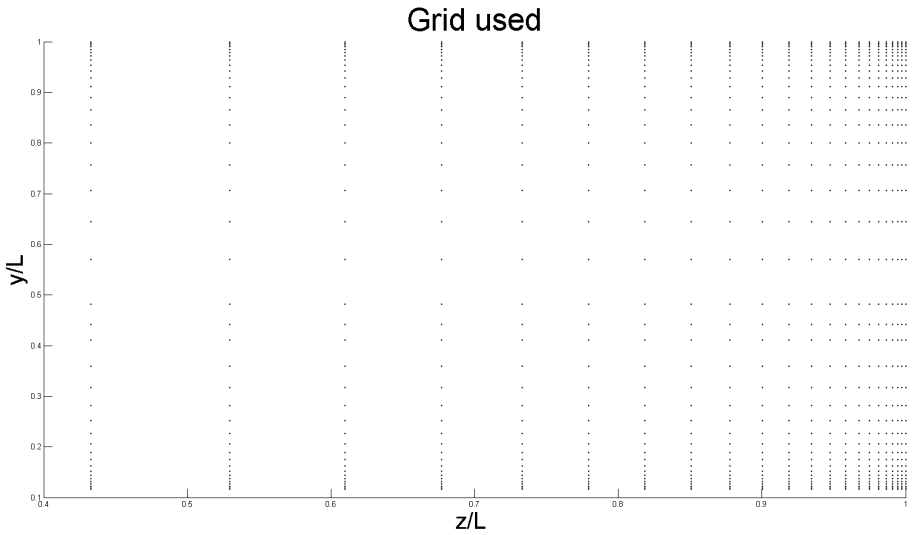

Figure 3.1: Grid used at the flow measurements

This is done for each case in the three different planes, changing the axial position. The first plane is situated at the same axial position as the trailing edge, another plane $x/L = 0.61$ from the trailing edge of the vane which is the farthest point reachable by the probe due to the vane shape. The other one is situated in between the two.

At the figures can be seen the vanes at the top and at the bottom, and the three planes with the different data. The trailing edge is situated at the 0 in the x axis, the sidewall is situated at the 120 in the z axis and the midplane is situated at the 72.5 in the x axis.

If the dynamic pressure is negative the velocity is undefined, in this graphs these undefined velocities will appear as velocity 0.

3.1 Static pressure

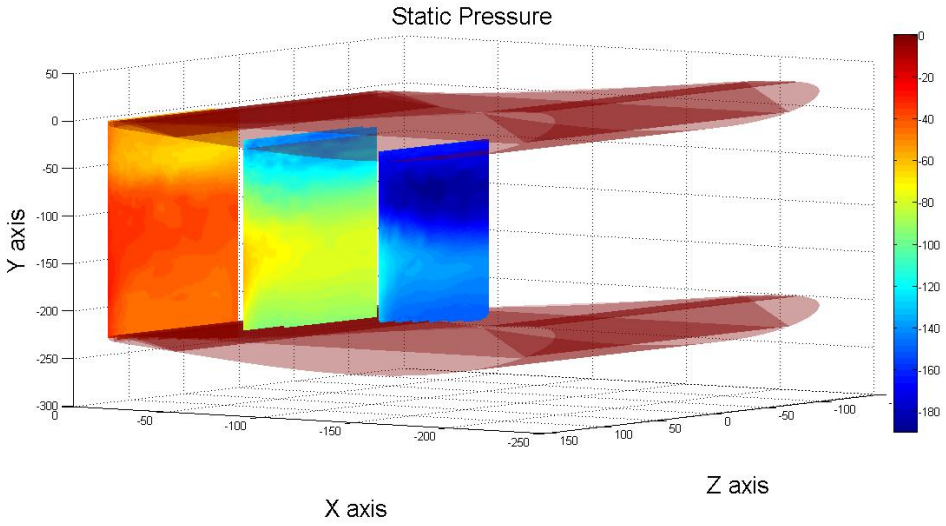

Figure 3.2: Static pressure at the three planes. Off-design -25 degrees. Re = 300000.

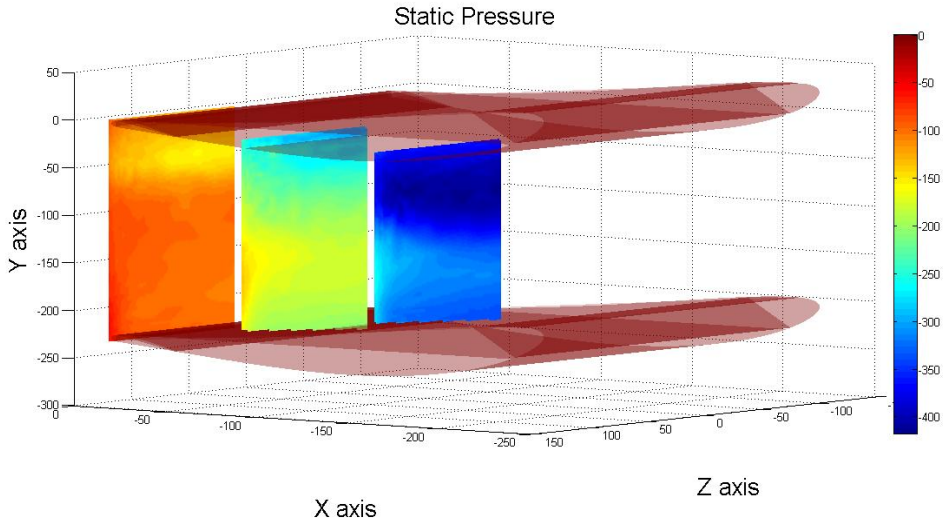

Figure 3.3: Static pressure at the three planes. Off-design -25 degrees Re = 450000.

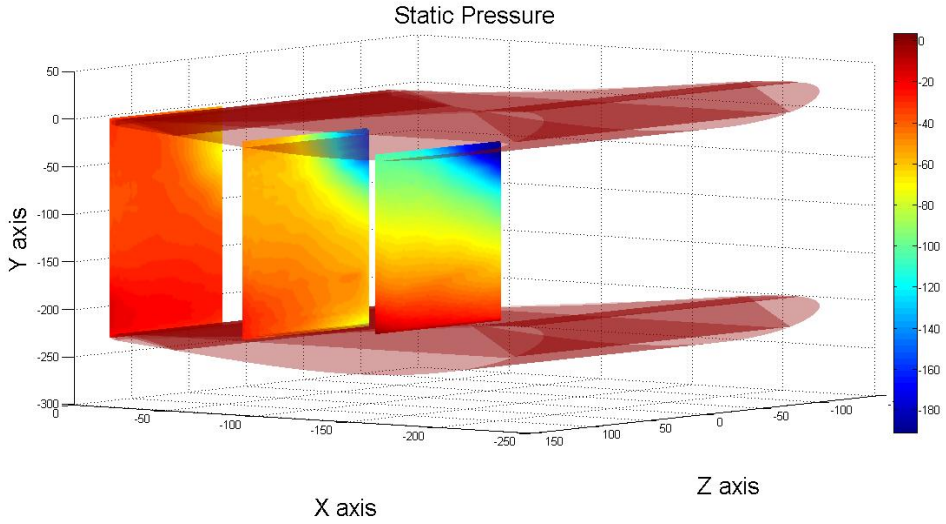

Figure 3.4: Static pressure at the three planes. Off-design 40 degrees. Re = 300000.

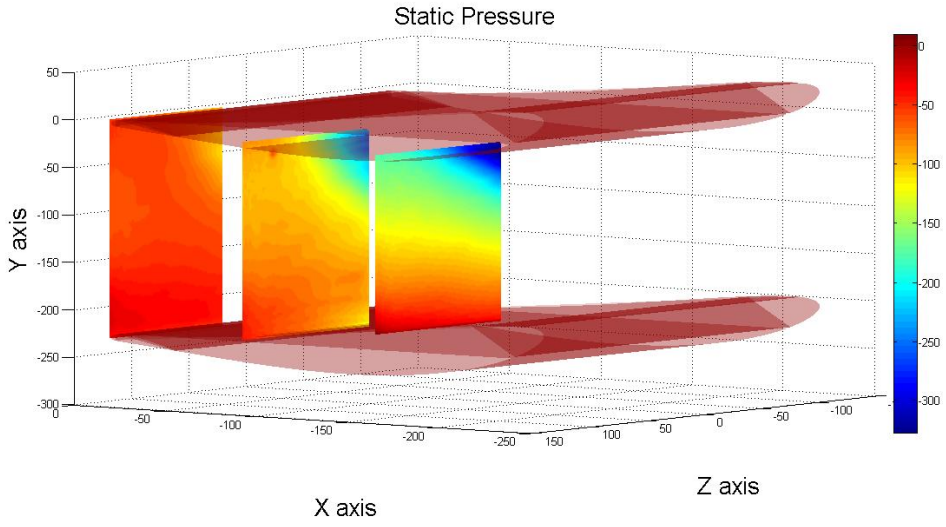

Figure 3.5: Static pressure at the three planes. Off-design 40 degrees. Re = 450000.

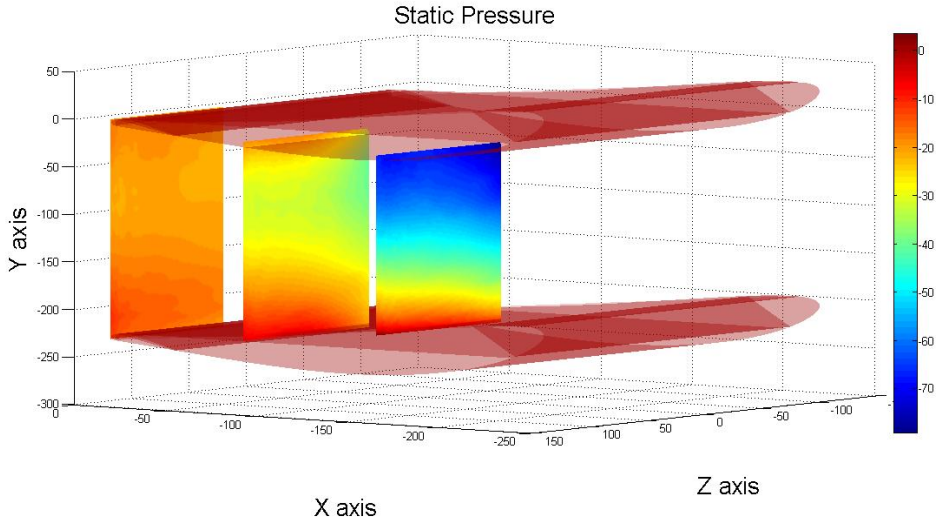

Figure 3.6: Static pressure at the three planes. On-design. Re = 300000.

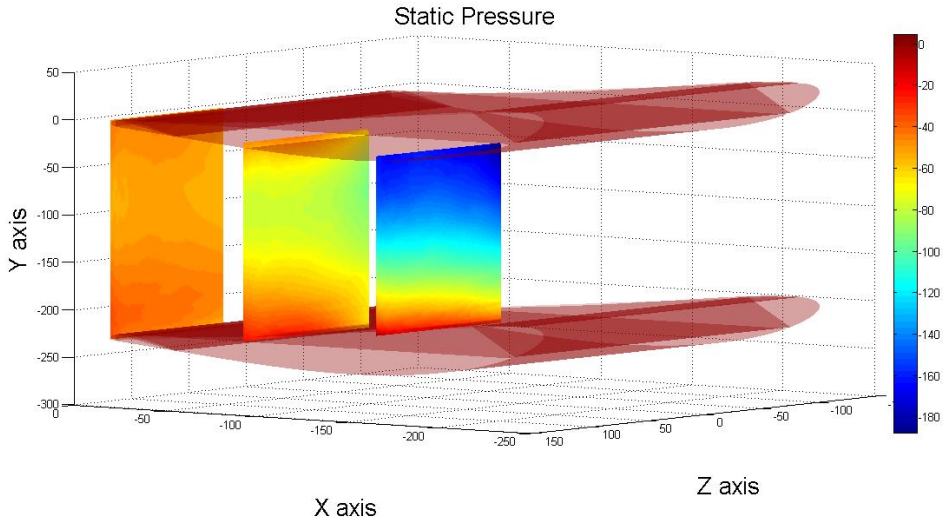

Figure 3.7: Static pressure at the three planes. On-design Re = 450000.

3.2 Total Pressure

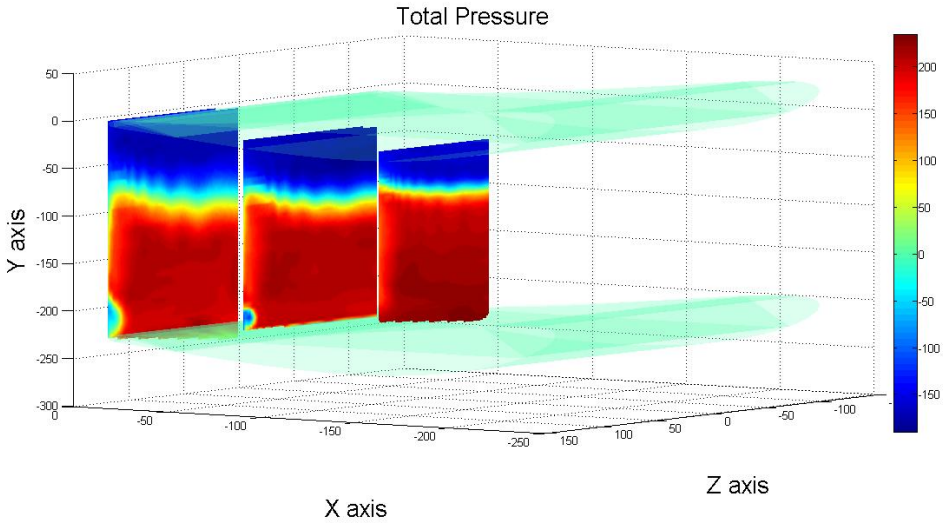

Figure 3.8: Total pressure at the three planes. Off-design -25 degrees. Re = 300000.

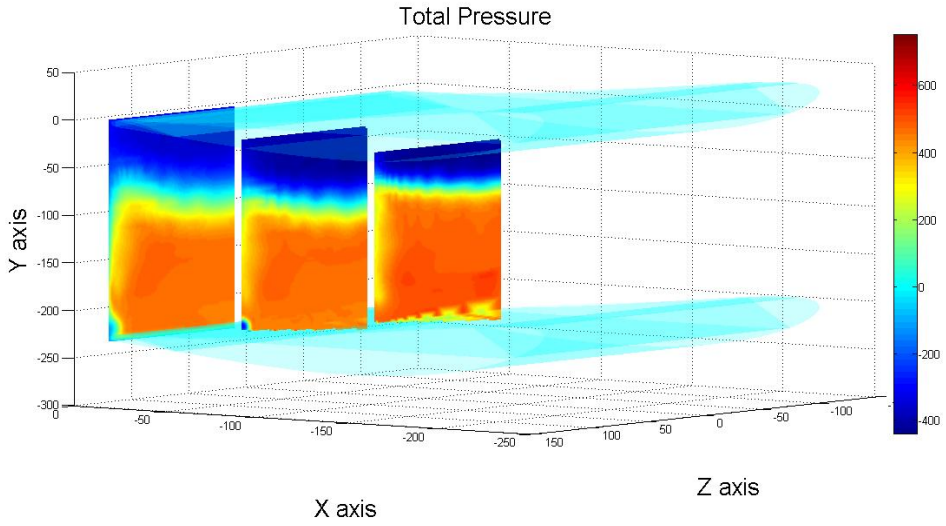

Figure 3.9: Total pressure at the three planes. Off-design -25 degrees. Re = 450000.

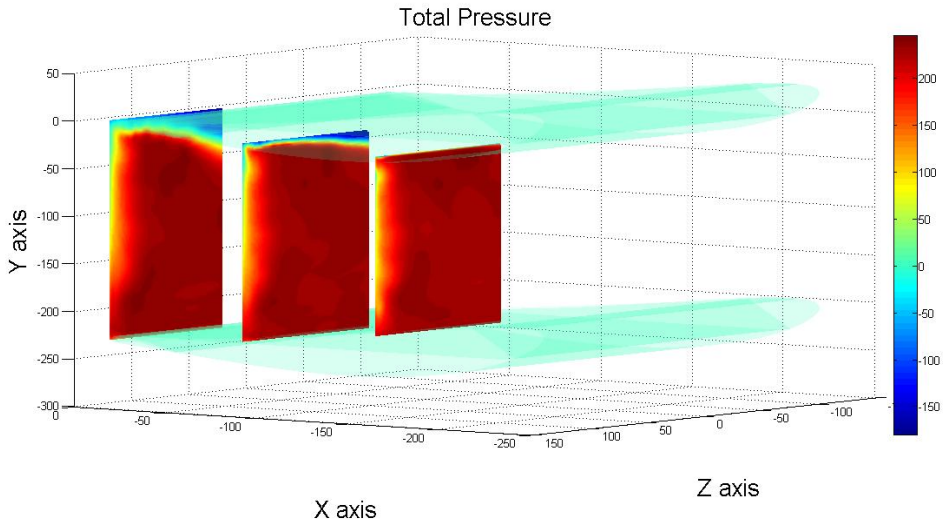

Figure 3.10: Total pressure at the three planes. Off-design 40 degrees. Re = 300000

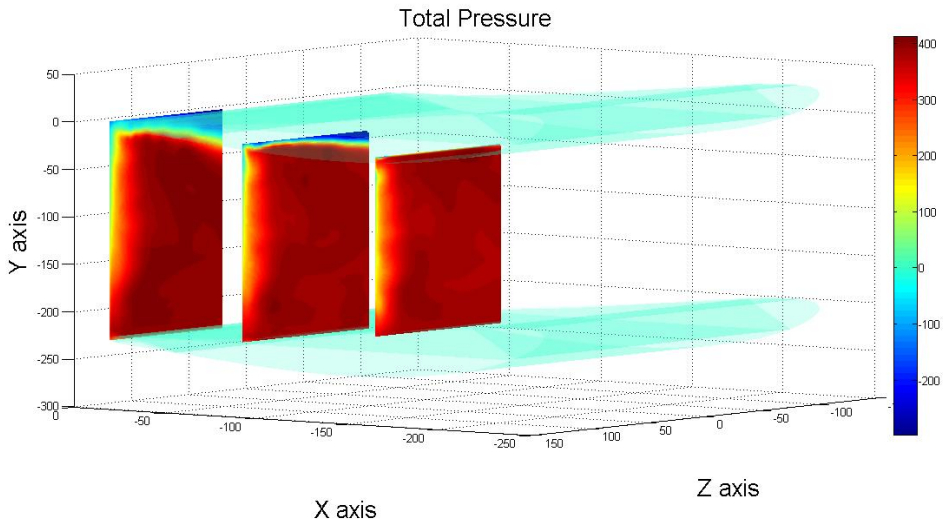

Figure 3.11: Total pressure at the three planes. Off-design 40 degrees. Re = 450000.

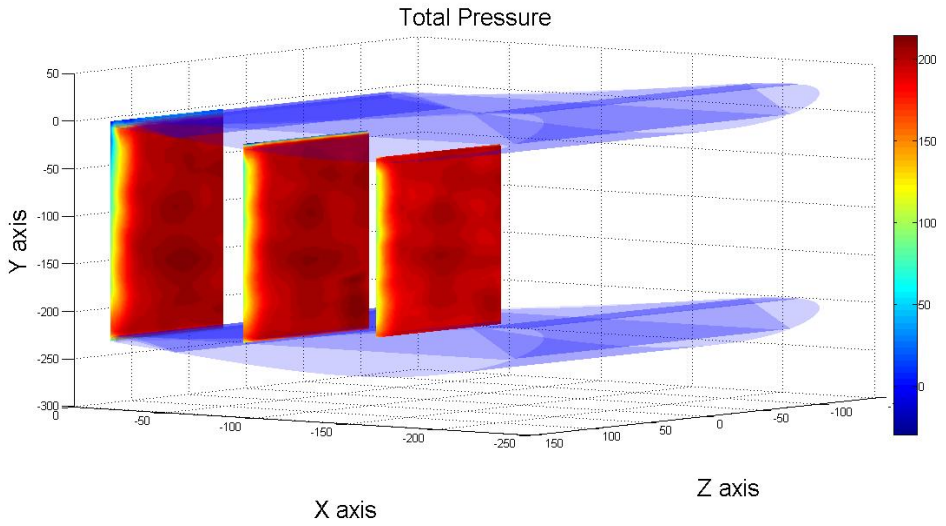

Figure 3.12: Total pressure at the three planes. On-design. Re = 300000.

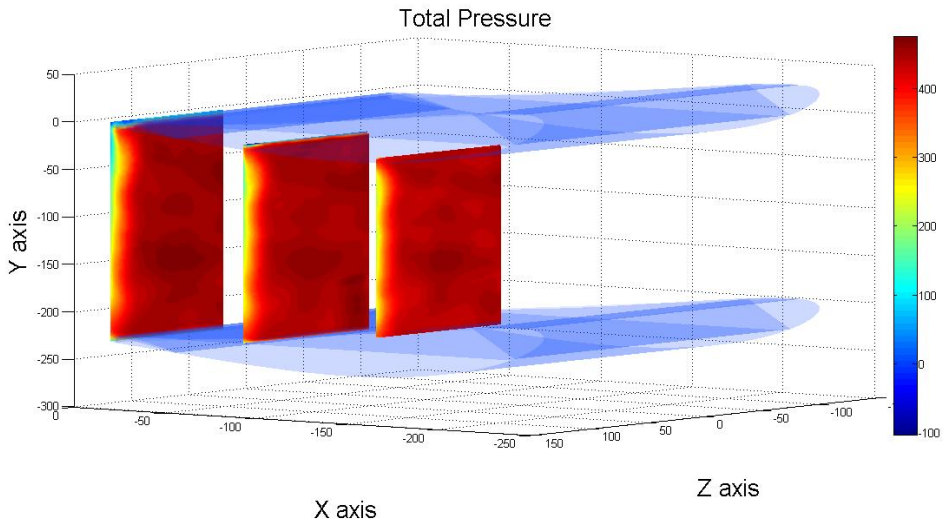

Figure 3.13: Total pressure at the three planes. On-design Re = 450000.

3.3 Velocity

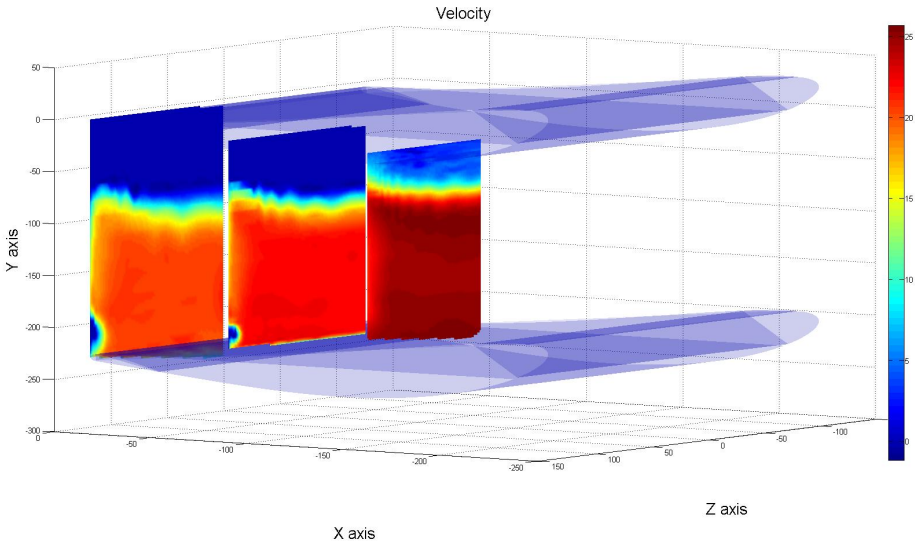

Figure 3.14: Velocity at the three planes. Off-design -25 degrees. Re = 300000

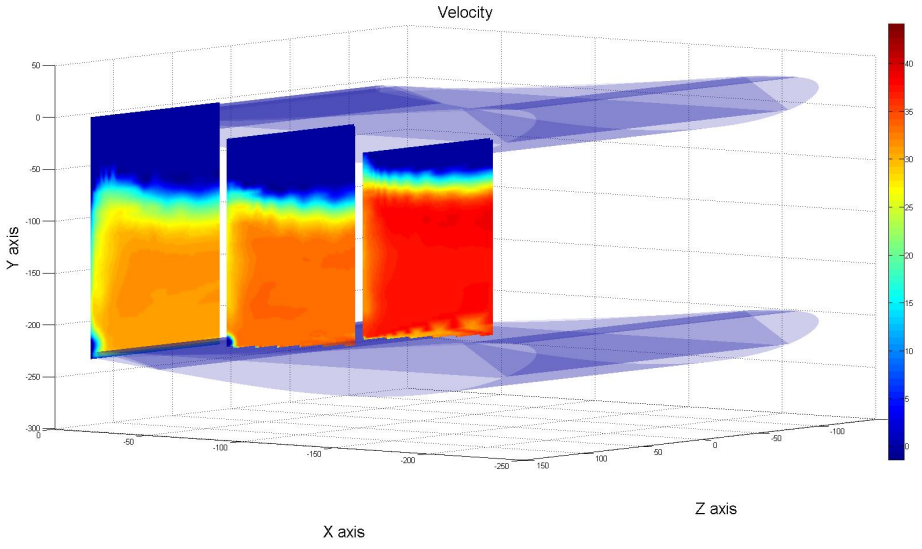

Figure 3.15: Velocity at the three planes. Off-design -25 degrees. Re = 450000.

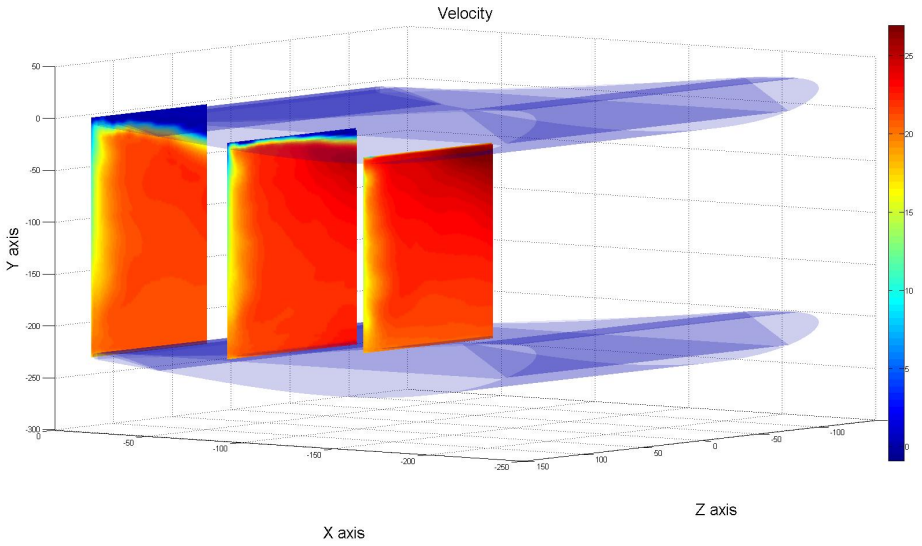

Figure 3.16: Velocity at the three planes. Off-design 40 degrees. Re = 300000

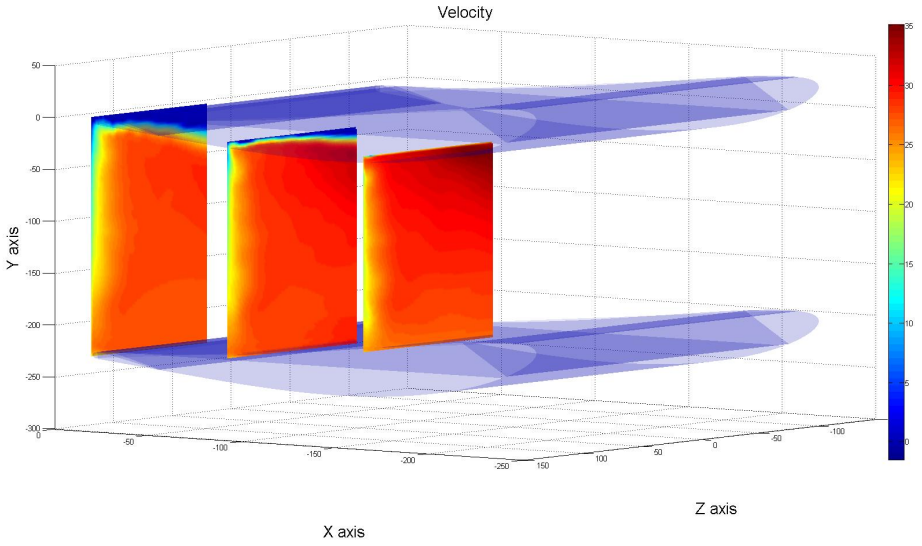

Figure 3.17: Velocity at the three planes. Off-design 40 degrees. Re = 450000.

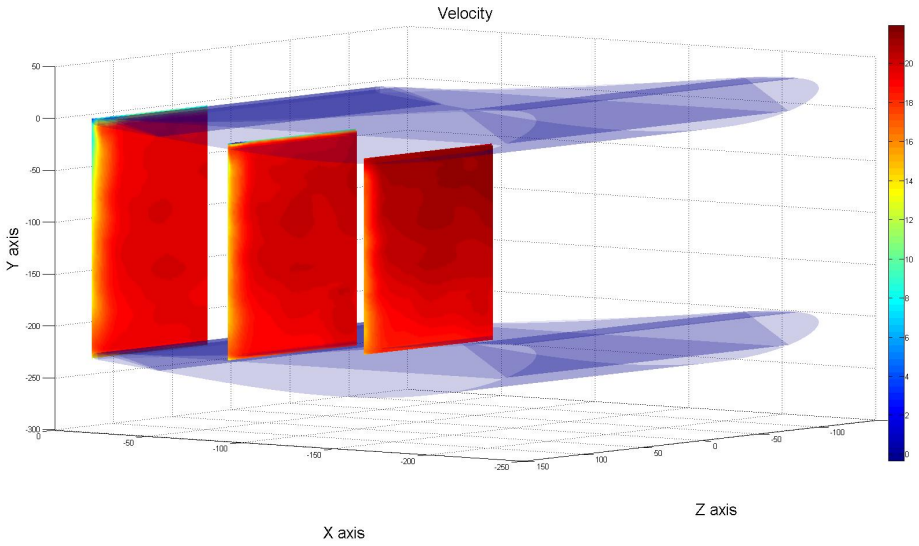

Figure 3.18: Velocity at the three planes. On-design. Re = 300000.

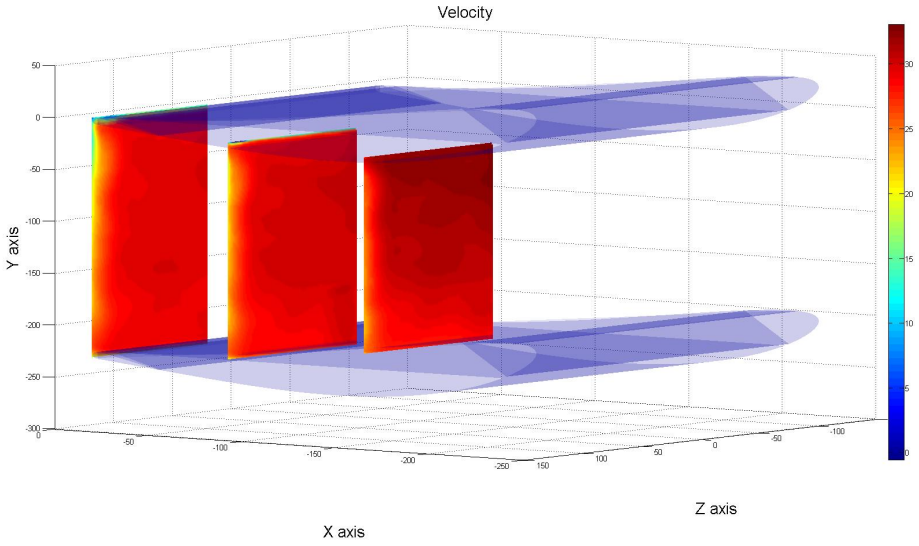

Figure 3.19: Velocity at the three planes. On-design Re = 450000.

This study shows the flow behaviour at different set ups, where the boundary layer is observed next to the end-wall and the vane surface. This is crucial to understand all the processes involved.

As expected, the Off-design cases show flow separation. In the off-design -25º case can be seen clearly the flow separation area, where there is a large area with recirculation. However, the on-design case shows an ideal behaviour where the air retains maximum velocity throughout the path.
This is a good point to start new more detailed studies. The data acquired from this experiment can be used to compare results from CFD simulations with the experimental data and, if both match, validate the CFD results.

4

Conclusions

The main achievement of this thesis is that a long-term instrument for heat transfer measurements on the end-wall for a linear cascade has been designed. Its defining features are that it allows parameters to be controlled and provides a possibility to obtain highly accurate results.

This new tool will give the department the possibility to study different cases in the linear cascade, both the mechanisms of heat transfer and the fluid mechanics involved. But due to delays in the manufacturing process of the end-wall, it was not possible to carry out any experiment, or verify the results obtained in the SolidWorks. However, the foundation is ready to perform the experiments and obtaining data.

Regarding the measurements, it can be concluded that there is enough data to observe the main flow structures and boundary layer sizes. Future work will be focused on the verification and validation of the CFD through the OGVs for heat transfer using the data that will be acquired with the instrumented end-wall and the flow measurement data.

5

Appendix

5.1 A.1

Plots of the temperature at the top surface of the aluminium plate at different cases.

5.1.1 Detailed results for 16 heaters.

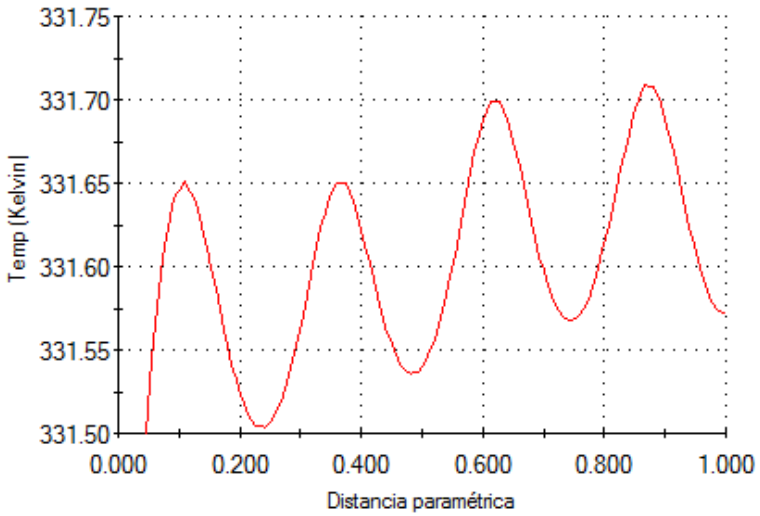

Figure 5.1: Temperature distribution along the top surface of aluminium plate with random heat flux power. 16 Heaters.

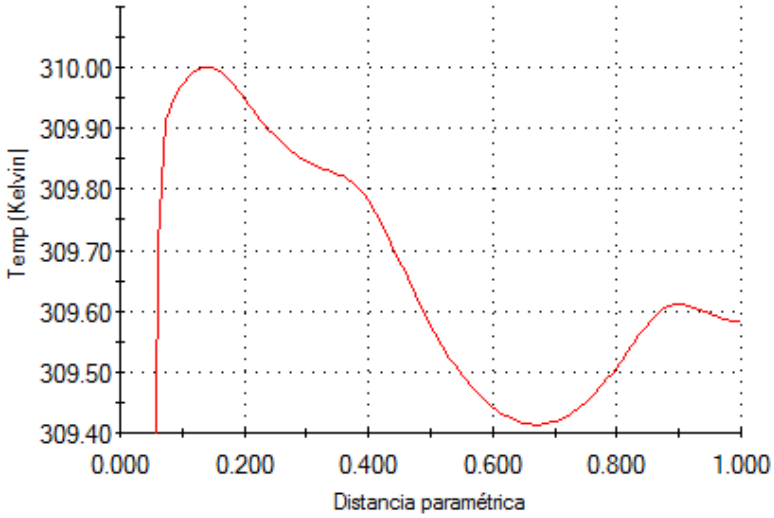

Figure 5.2: Temperature distribution along the top surface of aluminium plate without one heater. 16 Heaters.

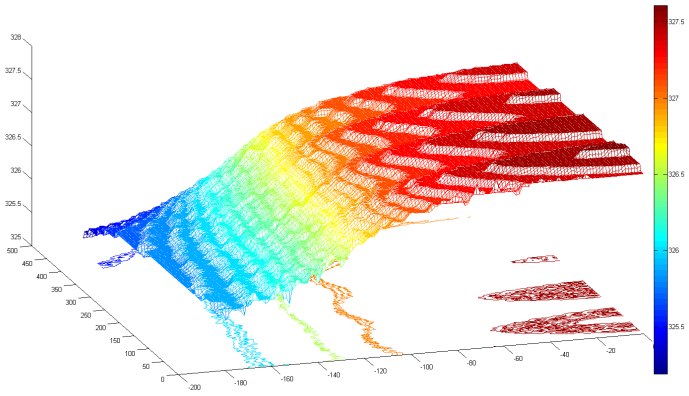

Figure 5.3: 3D temperature distribution along the top surface of aluminium plate. 16 Heaters.

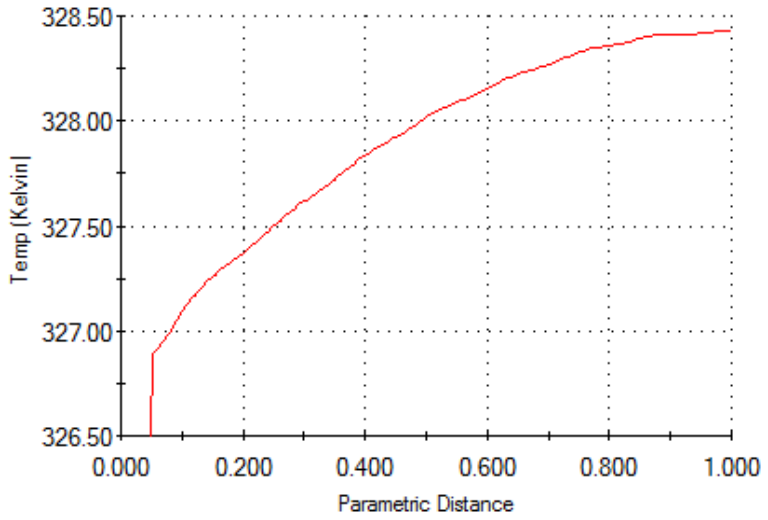

Figure 5.4: Temperature distribution along the top surface of aluminium plate with random heat flux power. 30 Heaters.

Detailed results for 30 heaters.

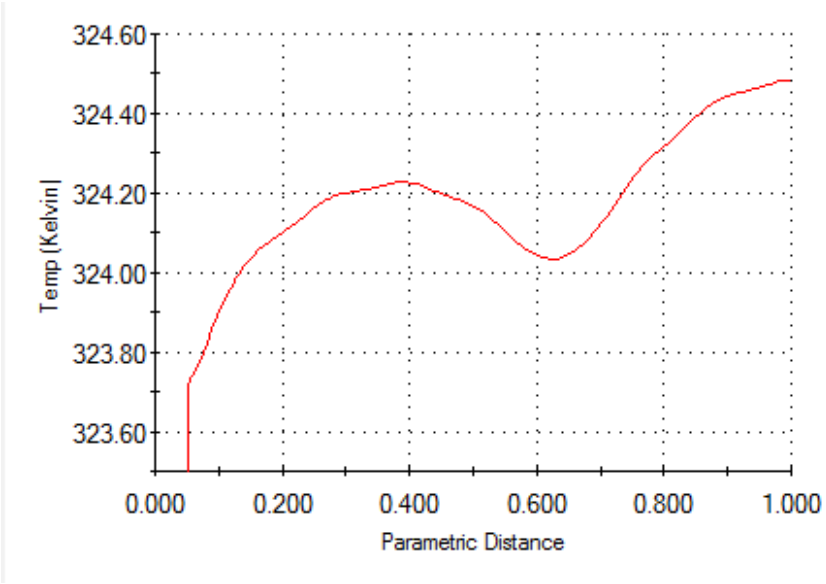

Figure 5.5: Temperature distribution along the top surface of aluminium plate without one heater. 30 Heaters.

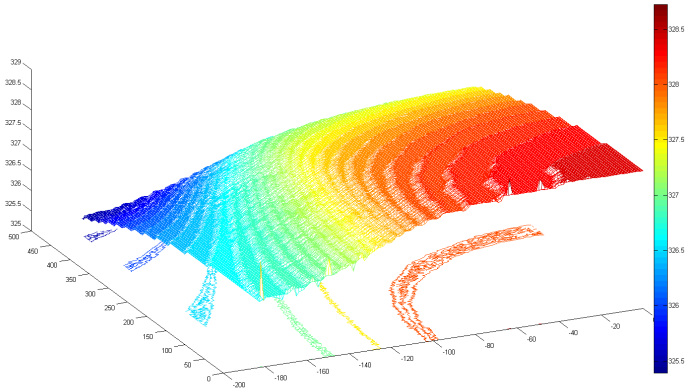

Figure 5.6: 3D temperature distribution along the top surface of aluminium plate. 30 Heaters.

5.2 A.2

Drawings of the window.

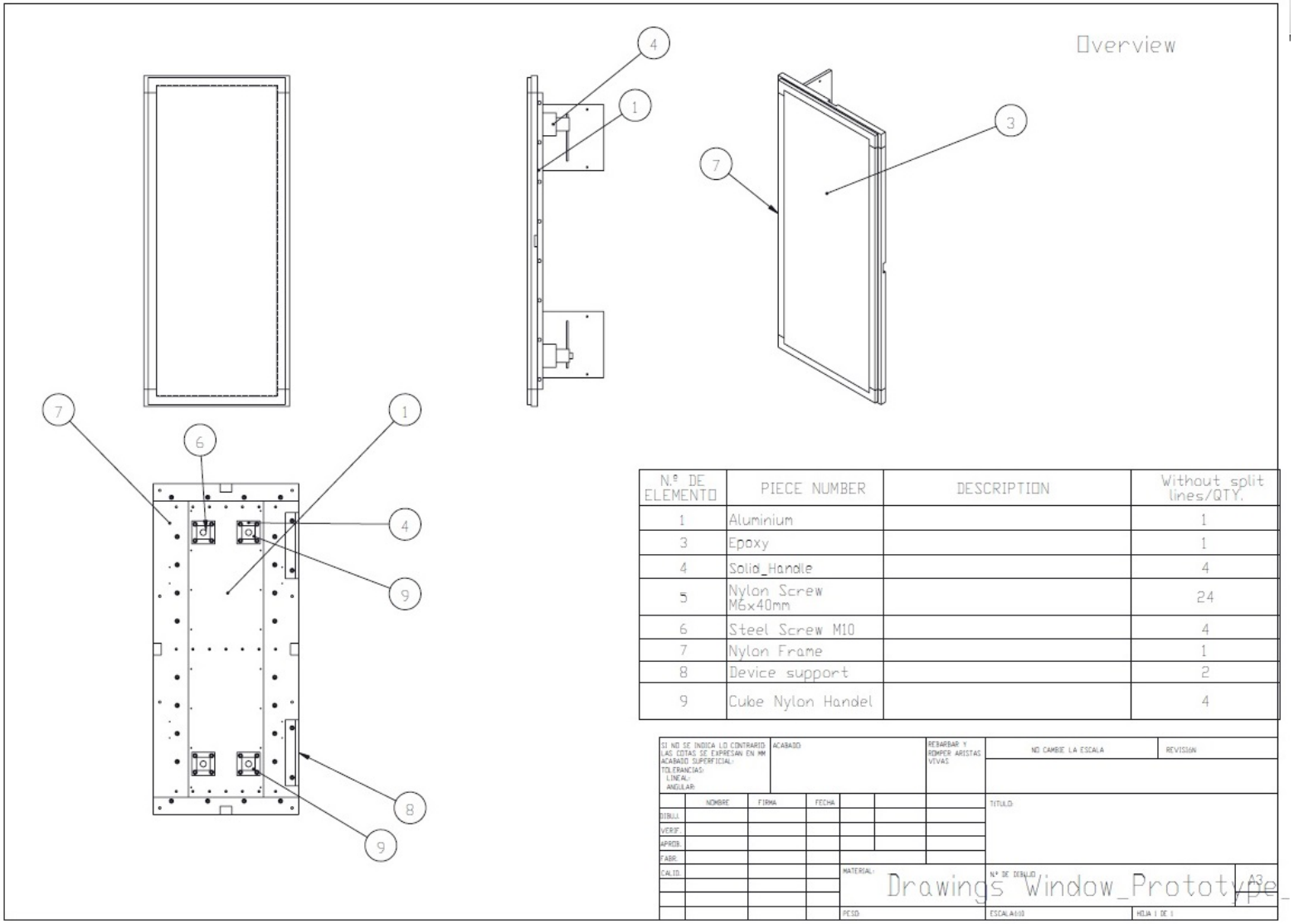

N.º DE ELEMENTO	PIECE NUMBER	DESCRIPTION	Without split lines/QTY.
1	Aluminium		1
3	Epoxy		1
4	Solid_Handle		4
5	Nylon Screw M6x40mm		24
6	Steel Screw M10		4
7	Nylon Frame		1
8	Device support		2
9	Cube Nylon Handel		4

Figure 5.7: Model overview

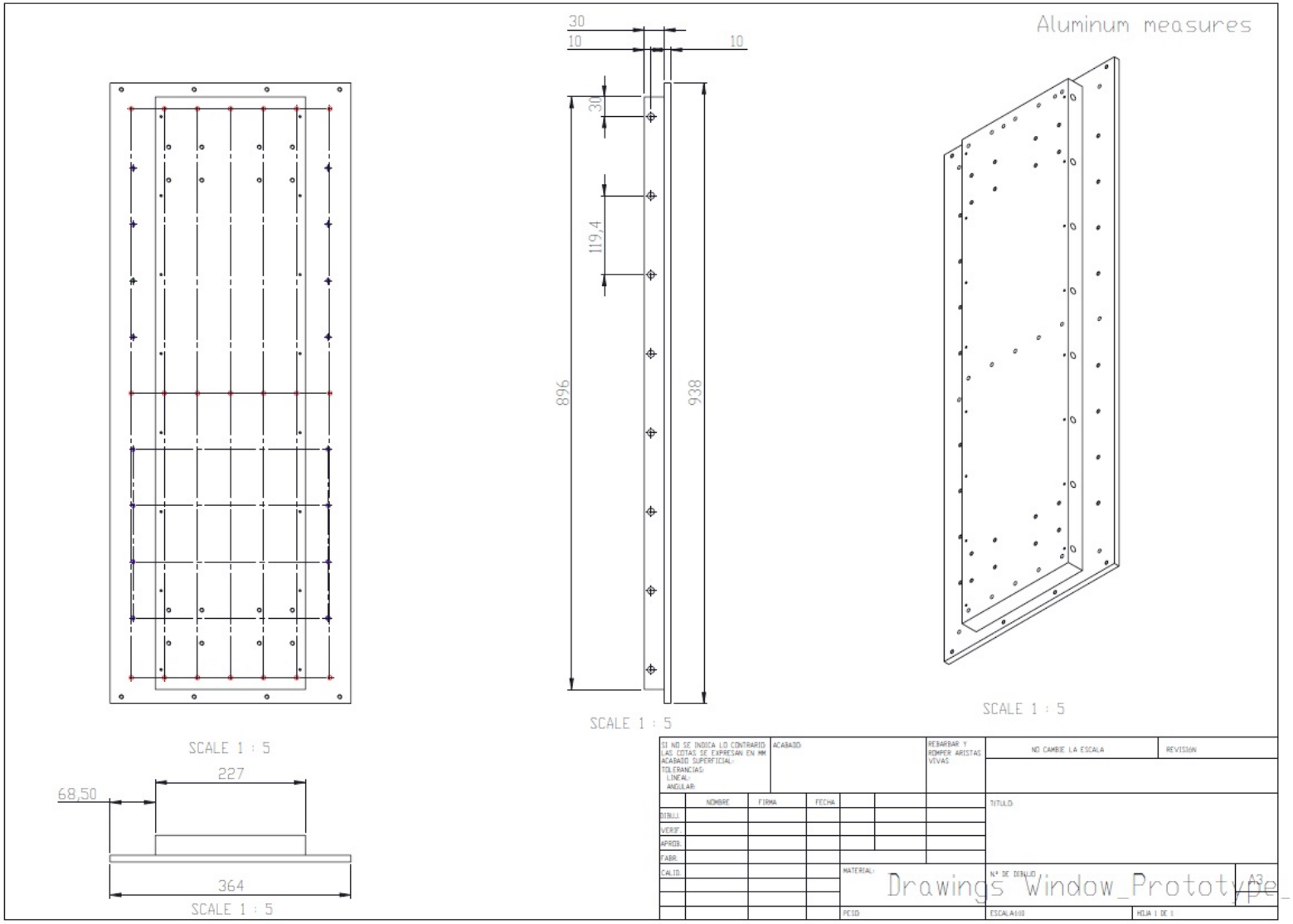

Figure 5.8: Aluminium overview

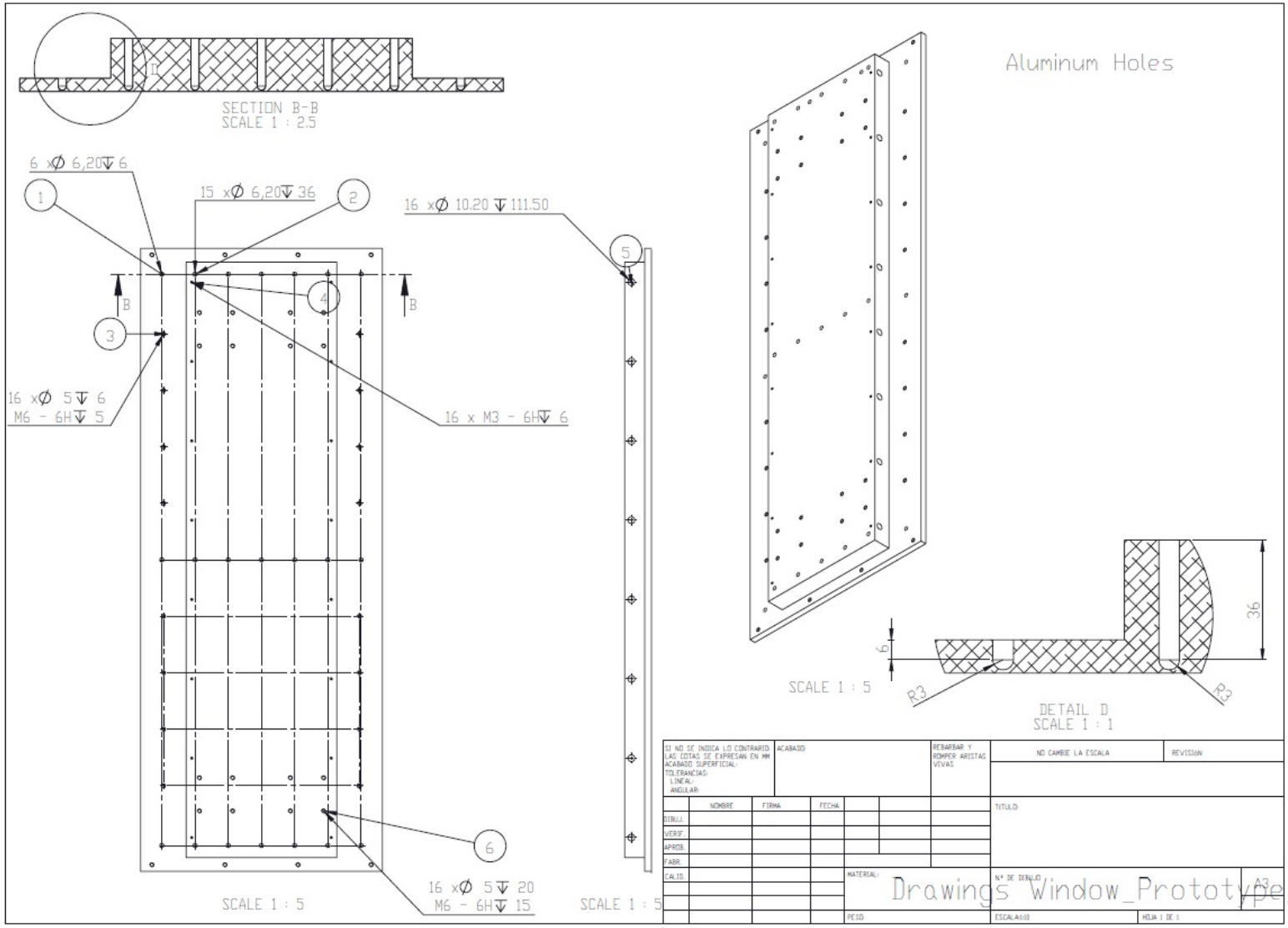

Figure 5.9: Holes at the alunium sheet

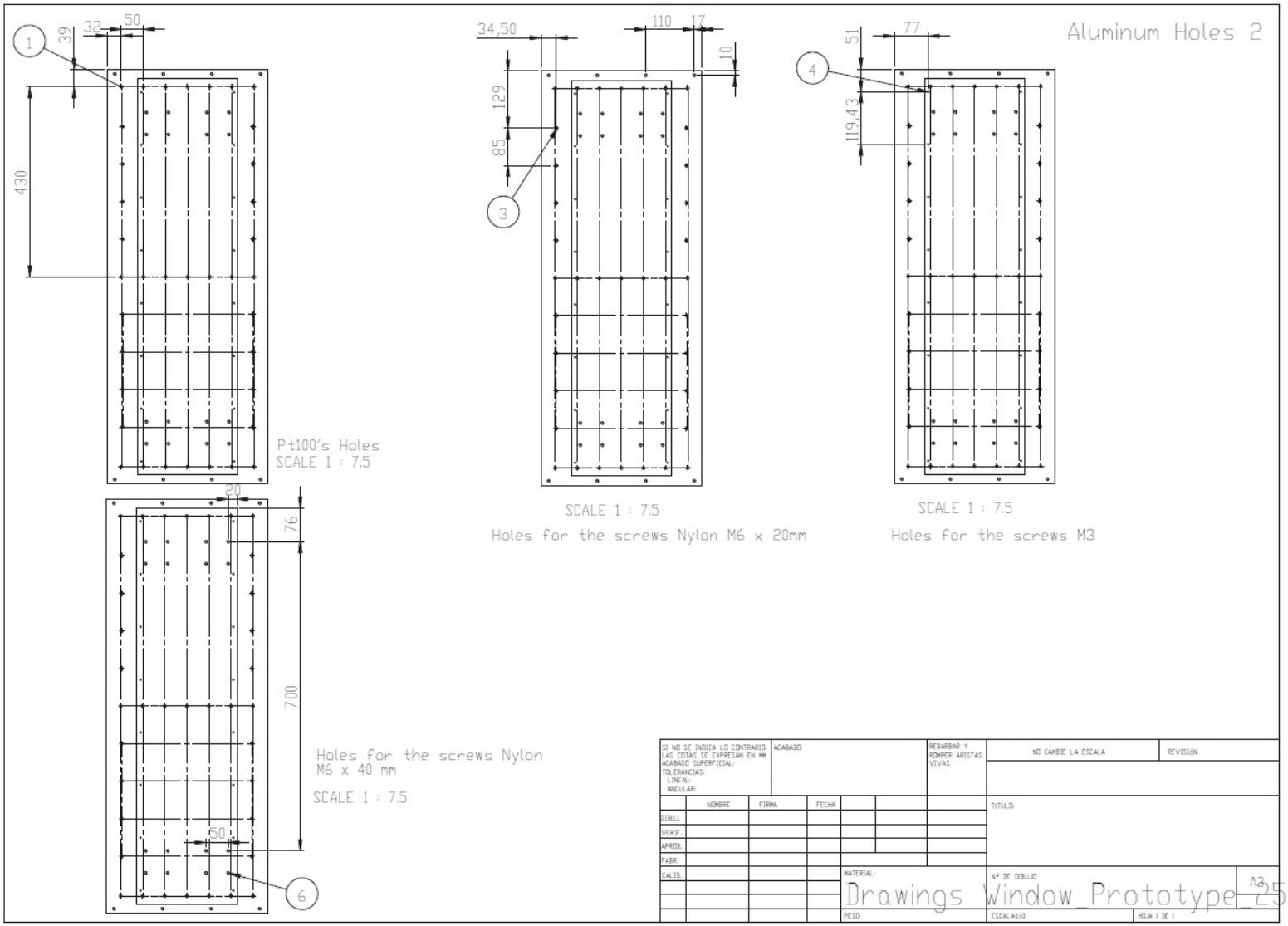

Figure 5.10: Holes at the aluminium sheet

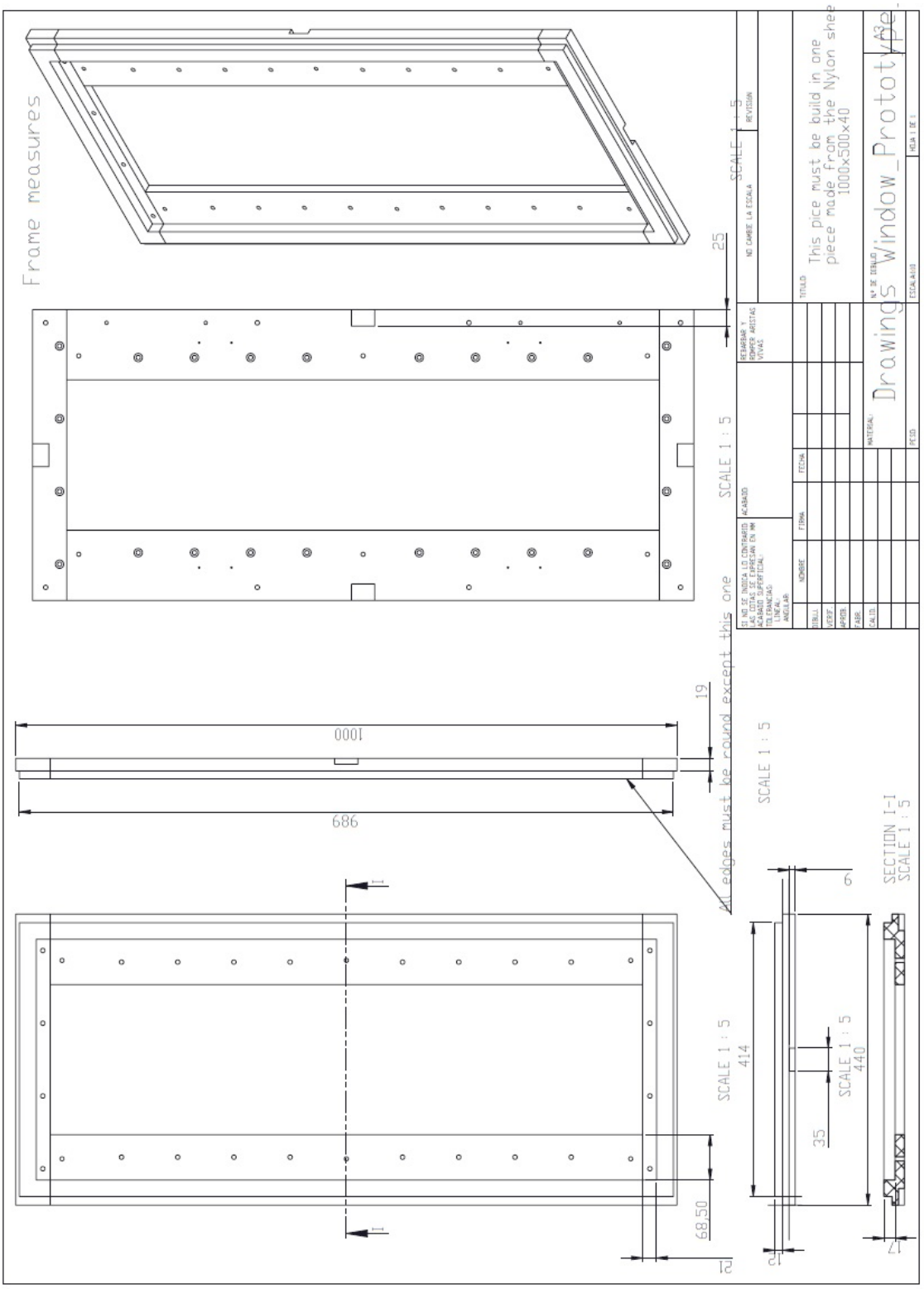

Figure 5.11: Frame overview

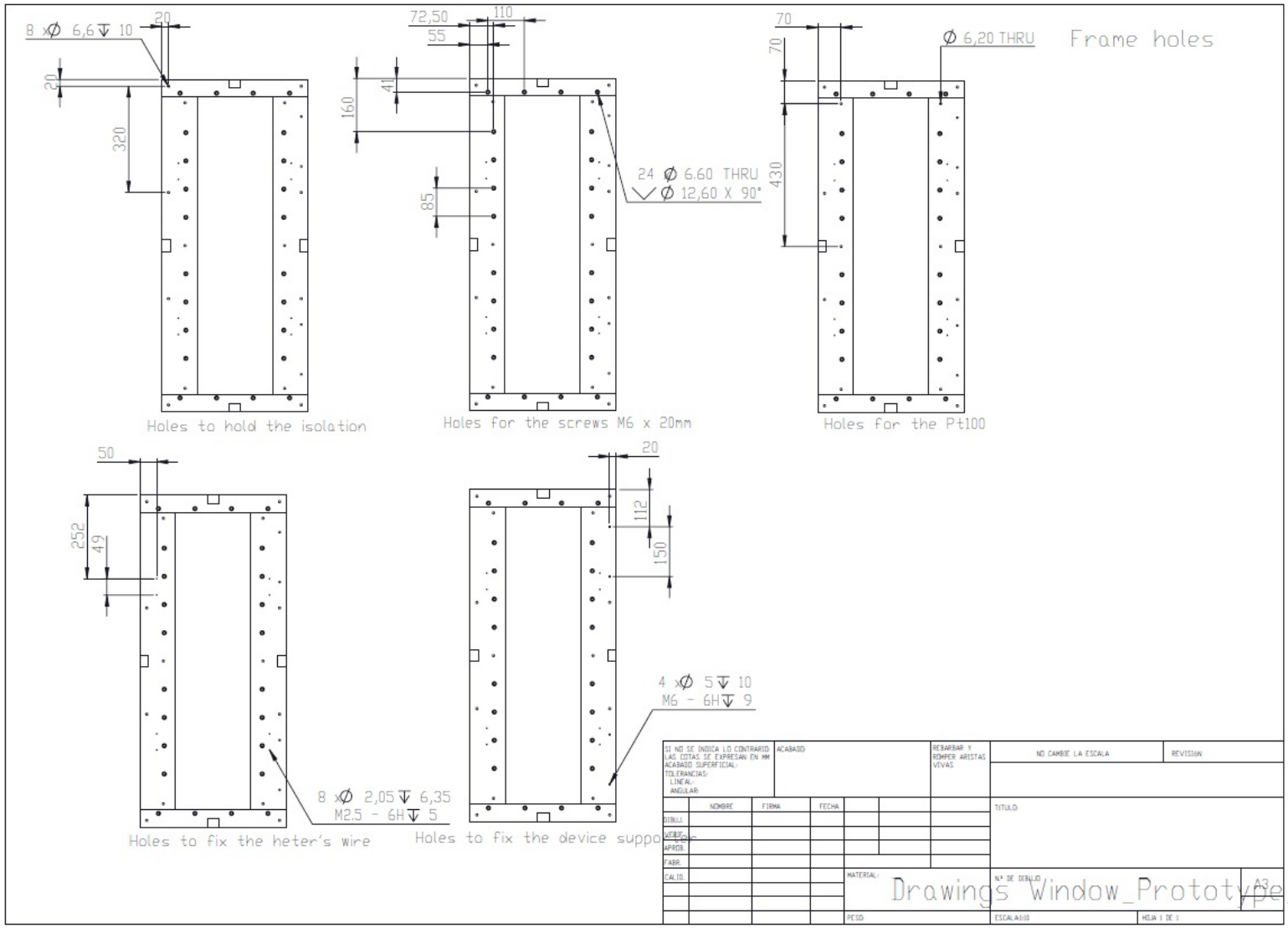

Figure 5.12: Frame holes

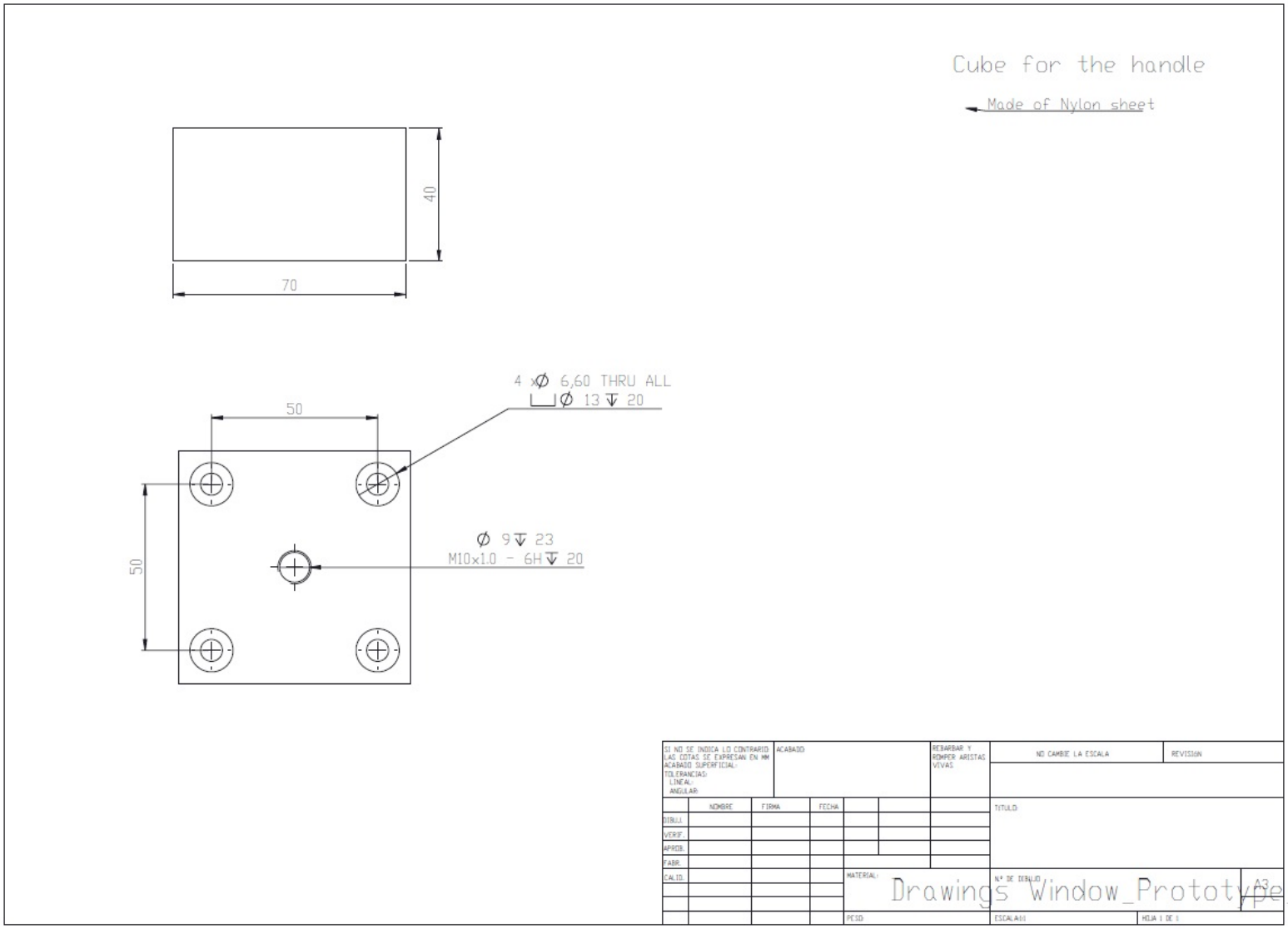

Figure 5.13: Nylon handle overview

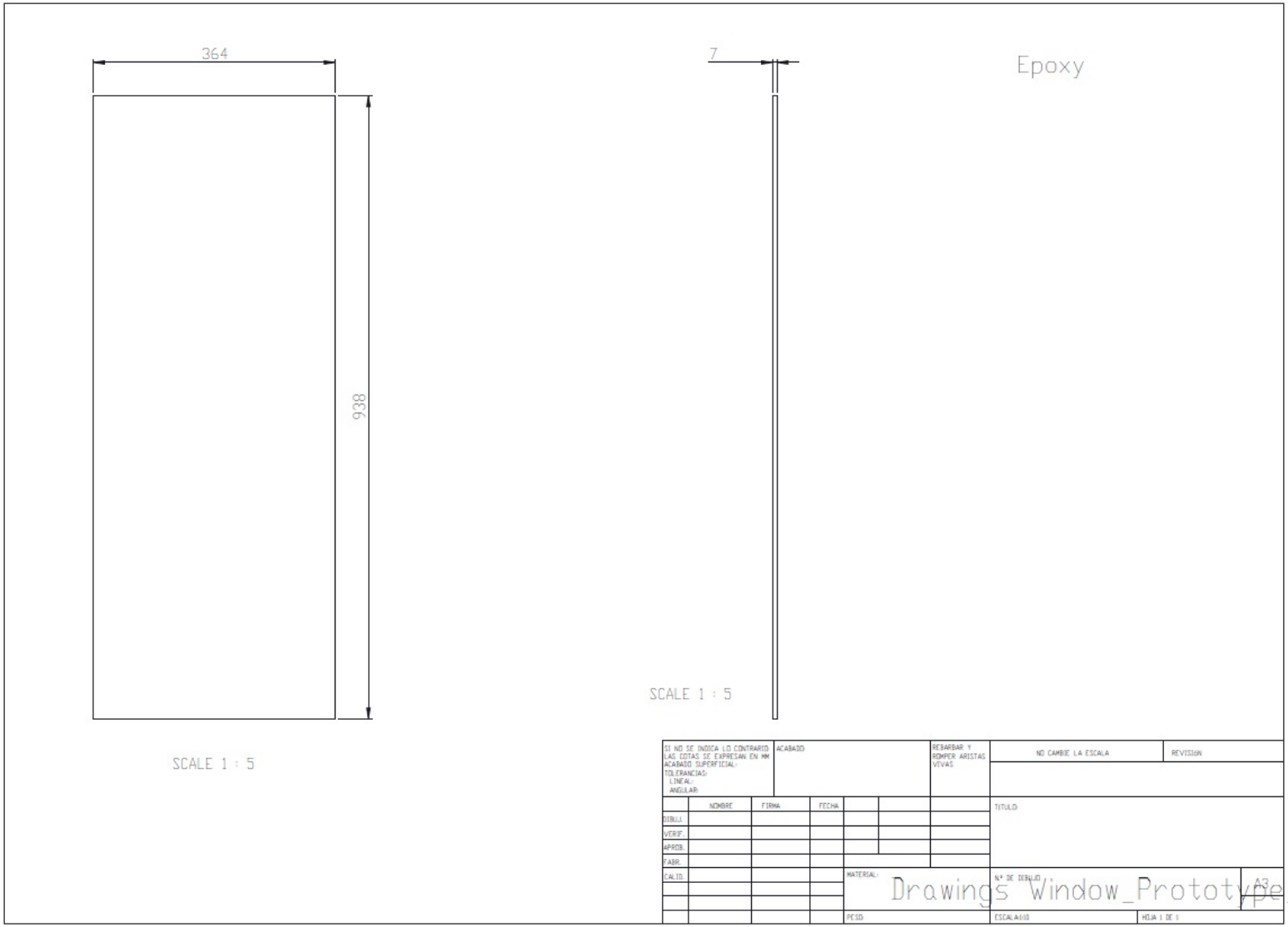

Figure 5.14: Epoxy overview

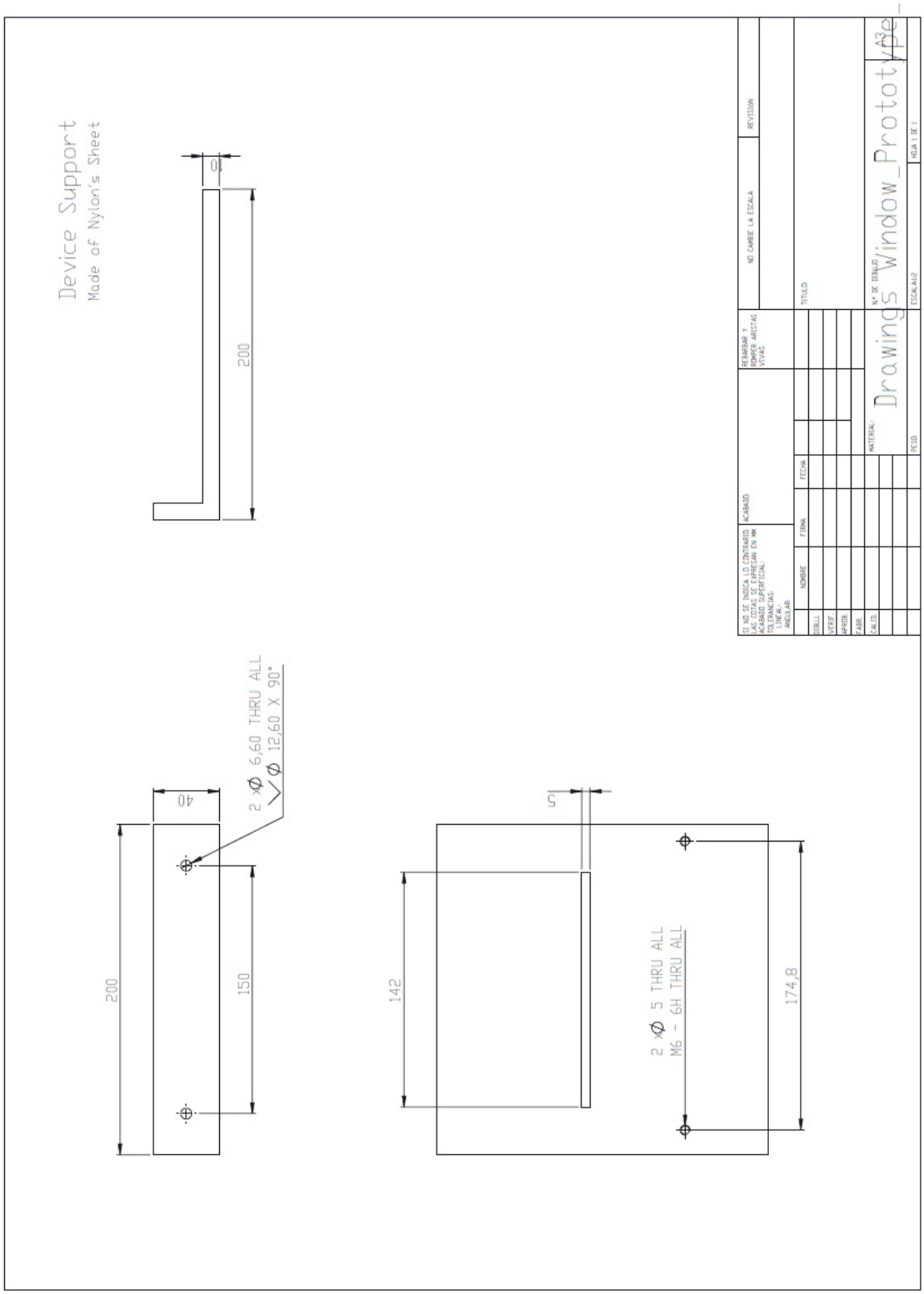

Figure 5.15: Device support

Figure 5.16: Nylon cube for handeling

List of Figures

Bibliography

[1] I. Kroo and J. Alonso, *Aircraft Design: Synthesis and Analysis*, Airfoil Pressure Distributions, (2005)
http://adg.stanford.edu/aa241/airfoils/airfoilpressures.html

[2] P. Kurowski, *"Thermal Analysis with SolidWorks Simulation 2014"*, (2014)

[3] P. Kurowski, *"Engineering Analysis with SolidWorks Simulation 2012"*, (2012)

[4] Matlab site, *R2014a Documentation*
http://www.mathworks.es/es/help/matlab/ref/mldivide.html

[5] Borja Rojo and C. Jimenez and V. Chernoray, *"Experimental Heat Transfer Study of Endwall in a Linear Cascade with IR Thermography"*, (2014)

[6] B. Rojo, *"Experimental Heat Transfer Study in Intermediate Turbine Duct"*, Master's Thesis in Solid and Fluid Mechanics, Chalmers University of Technology, (2012)

[7] M. Sanchotello and V. Orchillés, *"Transmissió de calor"* , (2005)

[8] C. Arroyo Osso, *"Aerothermal Investigation of an Intermediate Turbine Duct"*, Thesis for the Degree of Doctor of Philosophy, Chalmers Universityof Technology, (2009)

[9] Prof.Z.S Spakovszky, *"Thermodynamics and Propulsion"*, (2002)

[10] Rolls-Royce, *"Gas turbine technology"*, (2007).
*http : //www.rolls − royce.com/Images/gasturbines_tcm*92 − 4977.*pdf*

[11] C. Jimenez, *"Experimental Heat Transfer Study in Intermediate Turbine Duct"*, (2013).

[12] Incropera, DeWitt, Bergman, Lavine, *"Fundamentals of Heat and Mass Transfer"*,6^{th} Edition (2007).